The CSIRO Atmosphere Biosphere Land Exchange (CABLE) model for use in climate models and as an offline model

E. A. Kowalczyk, Y. P. Wang, R. M. Law, H. L. Davies,
J. L. McGregor and G. Abramowitz

The CSIRO Atmosphere Biosphere Land Exchange (CABLE) model for use in climate models and as an offline model

E. A. Kowalczyk, Y. P. Wang, R. M. Law, H. L. Davies,
J. L. McGregor and G. Abramowitz
CSIRO Marine and Atmospheric Research paper 013
November 2006

Abstract

Over the past twenty years, land surface models have developed from simple schemes to more complex representations of soil-vegetation-atmosphere interactions, allowing for linkages between terrestrial microclimate, plant physiology and hydrology. This evolution has been facilitated by advances in plant physiology and the availability of global fields of land surface parameters obtained from remote sensing. The CSIRO Atmosphere Biosphere Land Exchange (CABLE) model presented here calculates carbon, water and heat exchanges between the land surface and atmosphere and is suitable for use in climate models and in the form of a one-dimensional stand-alone model.

We provide a full description of CABLE and examples of offline and online simulations for selected sites. Online simulations are performed with CABLE coupled to the CSIRO Conformal-Cubic Atmospheric Model (C-CAM).

The model version presented here represents the first phase of a longer-term plan to improve the land surface schemes in the CSIRO and the Australian Community Earth System Simulator (ACCESS) global circulation models. This report is intended for users and future developers of CABLE.

Enquiries should be addressed to:
E. A. Kowalczyk
CSIRO Marine and Atmospheric Research
PMB 1, Aspendale, Victoria 3195, Australia
Phone: +61 3 9239 4524
Fax: +61 3 9239 4444
Email: eva.kowalczyk@csiro.au

Contents

1   Introduction

Atmospheric general circulation models (GCM) require a description of radiation, heat, water vapour and momentum fluxes across the land-surface atmosphere interface. Land surface schemes (LSS) are designed to calculate the temporal evolution of these fluxes, differentiating between bare ground and vegetation fluxes. The presence of vegetation affects climate by modifying the energy, momentum, and water balance of the land surface and changing atmospheric CO_2 concentrations. Associated with the effect of vegetation on climate, is the question of how the climate change may affect plant physiological properties and thus productivity. Increasing public interest in climate change has led to the need to develop more complete models of the climate system including the incorporation of the carbon cycle. In a coupled climate-carbon cycle model, plants affect climate and CO_2 concentrations while climate affects physiological parameters and productivity of plants. The CSIRO Atmosphere Biosphere Land Exchange (CABLE) LSS incorporates biogeochemical knowledge and is coupled with the CSIRO global Conformal Cubic Atmospheric Model (C-CAM) and elements of the terrestrial carbon cycle.

The biosphere atmosphere exchange model described in this technical paper represents Phase 1 of a long-term plan to improve the representation of surface processes in the CSIRO and ACCESS GCMs. The main purpose of the present technical paper is to provide a detailed description of CABLE.

2   Model history

The CSIRO land surface scheme has evolved from a simple scheme to a complex representation of biosphere atmosphere interaction. The main CSIRO GCM in 1990 had a single soil type, constant roughness length over land and no allowance for vegetation. It used the soil-moisture scheme of *Deardorff* [1977] and the force-restore method of *Deardorff* [1978] to calculate surface temperature. In 1991, a simple stand alone model of soil/canopy based on a big leaf description of a canopy and a force-restore model for soil was formulated by *Kowalczyk et al.* [1991]. The model was then implemented into the CSIRO GCM in 1993 as described in *Kowalczyk et al.* [1994]. The new scheme included a number of new features such as soil type (hence variable thermal and moisture properties), albedo, roughness length, canopy resistance, canopy interception of rainfall, runoff, deep soil percolation, snow accumulation and melting. The canopy was represented as a single vegetation layer with the characteristics of a large leaf acting as a source or sink of water vapour and sensible heat. The canopy temperature was calculated from the solution of the surface energy balance equation while the stomatal resistance was a function of radiation, saturation deficit, temperature and water stress.

In 1995 an improved version of soil/snow model was implemented into the CSIRO GCM and the CSIRO regional model, DARLAM (Division of Atmospheric Research Limited Area Model). The emphasis in the model development was to improve the seasonal simulation of soil moisture, heat cycles and snow cover. The multilayer soil model computed soil temperature and moisture differentiating between liquid water and ice content of the soil, whereas the new snow model was expanded to compute the temperature, snow density and thickness of three snowpack layers and a physically based snow albedo.

In 1997 the *Raupach et al.* [1997] Soil Canopy Atmosphere Model (SCAM) was developed as an offline version. SCAM included a canopy layer above the soil surface; formulation of an aerodynamic conductance for the turbulent transfer between soil, vegetation and atmosphere (accounting for turbulent exchanges within canopies) and responses of canopy stomata to radiation, saturation deficit, temperature and water stress. In 1998, SCAM was coupled to DARLAM

and was used to simulate energy fluxes measured during the CSIRO field program OASIS (Observations at Several Interacting Scales) as described in *Finkele et al.* [2003].

In 1998, a one layer two-leaf canopy model was formulated by *Wang and Leuning* [1998] on the basis of a multilayer model of *Leuning et al.* [1995]. A comparison of both one layer and multilayer model results showed consistency in the predictions of fluxes over a range of leaf area index values. Since the one layer model was ten times computationally more efficient than the multilayer model, it was more suitable for use in global circulation models. The one layer model differentiates between sunlit and shaded leaves, hence two sets of physical and physiological parameters were devised to represent the bulk properties of sunlit and shaded leaves. Several improvements were made to the one layer model, namely: allowance for non-spherical leaf distribution, an improved description of the exchange of solar and thermal radiation, and modification of the stomatal model of *Leuning et al.* [1995] to include the effects of soil water deficit on photosynthesis and respiration. The model was further refined by *Wang* [2000]. In 2003 the first version of CABLE which included the two-leaf canopy model, the canopy turbulence model and the multilayer soil/snow model was coupled with C-CAM. The subsequent addition of a simple carbon pool model to C-CAM, facilitated the completion of the Phase 1 C4MIP (Coupled Carbon Cycle Climate Model Intercomparison Project) experiment which required simulation of the twentieth century climate.

3   Model description

CABLE is a model of biosphere atmosphere exchange allowing for interaction between microclimate, plant physiology and hydrology.

The main features of CABLE are:

1. The vegetation is placed above the ground allowing for full aerodynamic and radiative interaction between vegetation and the ground.

2. A coupled model of stomatal conductance, photosynthesis and partitioning of absorbed net radiation into latent and sensible heat fluxes.

3. The model differentiates between sunlit and shaded leaves i.e. two-big-leaf submodel for calculation of photosynthesis, stomatal conductance and leaf temperature.

4. The radiation submodel calculates the photosynthetically active radiation (PAR), near infrared and thermal radiation.

5. The plant turbulence model by *Raupach et al.* [1997] is used to calculate air temperature and humidity within the canopy.

6. Annual plant net primary productivity is determined from the annual carbon assimilation corrected for respiratory losses. The seasonal growth/decay of biomass is determined by partitioning of the assimilation product between leaves, roots and wood. The flow of carbon between the vegetation and soil is described at present by a simple carbon pool model [*Dickinson et al.*, 1998].

7. A multilayer soil model is used. The Richards' equation is solved for soil moisture while the heat conduction equation is used for soil temperature.

8. The snow model computes the temperature, density and thickness of three snowpack layers.

CABLE consists of a number of submodels: (a) canopy processes, (b) soil and snow, (c) carbon pool dynamics and soil respiration.

3.1 Basic formulations for land surface processes.

CABLE calculates the temporal evolution of CO_2, radiation, heat, water and momentum fluxes at the surface. The vertical eddy fluxes of heat, water and momentum are dependent on the mean properties of the flow through the use of aerodynamic resistances. The general form for the sensible and latent heat fluxes is

$$H / \rho_a \, c_p = \overline{w'T'} = -u_* T_* = (T_{\text{sur}} - T_{\text{ref}})/r_H, \tag{1}$$

$$E / \rho_a = \overline{w'q'} = -u_* q_* = (q_{\text{sur}} - q_{\text{ref}})/r_E. \tag{2}$$

T_{ref} and q_{ref} are air temperature and specific humidity at the reference level, and T_{sur} and q_{sur} are surface values, ρ_a is air density, c_p is the specific heat, u_*, T_*, q_* are turbulent scales for velocity, temperature and humidity, r_H is aerodynamic resistance for heat and r_E the resistance for water exchange between the surface and a reference level, $\overline{w'T'}$ is the turbulent heat flux and $\overline{w'q'}$ is the turbulent moisture flux. r_E comprises aerodynamic as well as plant stomatal resistance. Knowledge of surface temperature T_{sur} is required for the computation of fluxes. T_{sur} is obtained through the closure of the energy balance at the lower atmosphere boundary which is one of the main tasks of the land surface scheme. The energy balance equation is solved for the temperature of the surface which may consist of a combination of surface elements such as vegetation, bare ground, snow and ice. The energy balance for any particular surface is written here as:

$$R_n - G = H + \lambda E \tag{3}$$

where R_n is the net radiation flux at the surface, G is the thermal storage flux (negligible for vegetation), with the sum of the latent (λE) and the sensible (H) heat fluxes defining the available energy. In CABLE the vegetation is placed above the ground allowing for full aerodynamic and radiative interaction between the vegetation and the ground. Hence the total surface fluxes for the combined canopy ground system are the sum of the fluxes from the soil (*s*) to the canopy air space and the fluxes from the canopy (*c*) to the atmosphere:

$$H_T = H_s + H_c, \tag{4}$$

$$\lambda E_T = \lambda E_s + \lambda E_c. \tag{5}$$

Central to the calculation of surface fluxes is the parameterization of aerodynamic resistances which depends on the reference level for the atmospheric variables T and q and the description of canopy aerodynamics. *Raupach et al.* [1997] developed a sophisticated description of single-layer canopy aerodynamics, including treatment of canopy turbulence (see section 3.1.2). He used *Monin and Obukhov* [1954] similarity theory for the parameterization of the surface fluxes for a combined canopy ground system. In the Monin-Obukhov theory the lowest model level lies in the surface layer within which the surface fluxes are constant in the vertical. Integrating

the flux-profile relationship between the roughness length, z_0, and the height of the first model level, z, results the following relationship [*Louis*, 1979]:

$$u(z) = \frac{u_*}{k} [\, \ln(z/z_0) - \psi_M(z/L_{MO}) + \psi_M(\, z_0/L_{MO}) \,],$$

hence the expression for the friction velocity can be written as:

$$u_* = \frac{k U_{\text{ref}}}{\ln(z_{\text{ref}}/z_0) - \psi_M(\xi) + \psi_M(\xi\, z_0/z_{\text{ref}})} \tag{6}$$

where z_{ref} is the first model level (reference level), U_{ref} is the mean wind at the reference level, k is the von Karman constant (0.4), ψ_M is Businger-Dyer functions for the flux-profile relationships for momentum for both stable and unstable conditions, L_{MO} is the Monin-Obukhov stability height, and ξ is a nondimensional height.

In order to calculate the friction velocity the nondimensional height ξ, which is a thermal stability parameter, must be computed:

$$\xi = \frac{z_{\text{ref}}}{L_{MO}} \tag{7}$$

where L_{MO} is defined as [*Garratt*, 1992]:

$$L_{MO} = -u_*^3 \, / \, (\, k\, (g/T)\, \overline{w'T'}) = -u_*^3 \, / \, (\, k\, g\, H_T / (\, T\, \rho_a\, c_p)\,) \tag{8}$$

where k is the von Karman constant, g is the gravity constant and $\overline{w'T'}$ the turbulent heat flux. Substituting Eq. 8 to Eq. 7 and adding a fraction of the latent heat flux (*Raupach et al.* [1997] Sec. 3.9) gives us the formula for the stability parameter used in CABLE:

$$\xi = -z_{\text{ref}}\, k\, g\, (\, H_T\, +\, 0.07\, \lambda E_T\,)\, / \, (\, T_{\text{ref}}\, \rho_a\, c_p\, u_*^3\,) \tag{9}$$

with H_T and λE_T being total grid fluxes as defined in Eqs. 4 and 5.

The calculation of fluxes, and hence ξ, depends strongly on the surface temperature but simultaneously the surface temperature depends on ξ, hence, an iteration method is used to allow for simultaneous calculation of all the required variables using values from the current time step. At the start, neutral stability is assumed so $\xi = 0$, $T_c = T_{\text{ref}}$ and $q_c = q_{\text{ref}}$. After computation of the resistances, fluxes and canopy temperature, a new value of ξ is obtained from Eq. (9). The iteration is repeated with the new value of ξ. Four iterations are used to obtain final values of the stability parameter, surface fluxes and canopy temperature.

3.1.1   Model structure

An iterative procedure, used for the simultaneous calculations of the stability parameter, fluxes and vegetation temperature, imposes a specific model structure where the calculations independent of the stability parameter are performed outside of the iteration loop. The basic flow diagram of CABLE is presented in Fig.1, with the stability iteration loop clearly depicted.
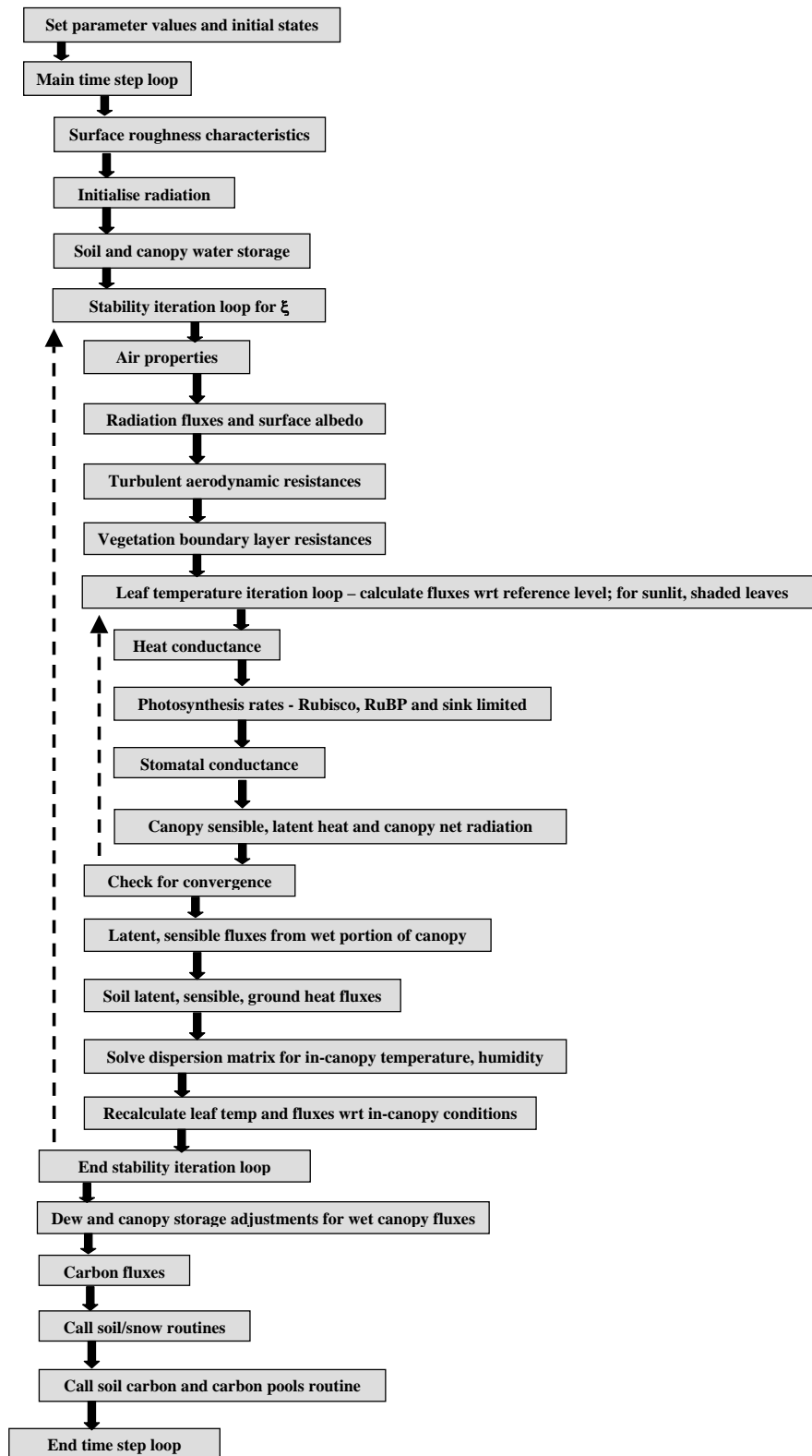
Figure 1: Flow diagram of CABLE.

At the beginning of a time step the following calculations are performed: initialisation of some of the radiation terms, evaluation of the canopy and soil water storage from the previous time step values and calculation of surface roughness characteristics. In CABLE the roughness length of vegetation is a function of canopy height and leaf area index [*Raupach*, 1994], the latter varying on a daily basis. The roughness length of the ground is for the transfer from the ground to the in-canopy air space, hence the values are smaller than the typical values used in other land surface schemes in which roughness length directly depends on the height of the roughness element.

At each iteration loop, first the fluxes are calculated *with reference to* (denoted by "wrt" on the diagram) the first model level, then Localised Near Field (LNF) theory [*Raupach*, 1989a, b] is used for the in-canopy temperature and humidity, before the fluxes are recalculated with reference to the in-canopy variables. A detailed description of the LFN theory application in canopy modelling is given in section 3.3 of *Raupach et al.* [1997]. All of the variables calculated within the stability loop are diagnostic, i.e. they are solutions of various algebraic equations which are functions of the current step atmospheric forcing, soil heat and water stores. The stability iteration loop includes the calculation of:

1. Air properties.

2. Radiation fluxes for canopy and soil, section 3.2.1.

3. Aerodynamic properties, section 3.1.2.

4. Vegetation boundary layer resistances [*Leuning et al.*, 1995] .

5. Solution of the coupled model of stomatal conductance, photosynthesis and partitioning of net available energy, depicted on the diagram as leaf iteration loop, section 3.2.3 .

6. Wet canopy fluxes.

7. Soil latent, sensible and ground heat fluxes, section 3.3.1.

8. Solution of the dispersion matrix [*Raupach et al.*, 1997].

9. Recalculation of fluxes with reference to in-canopy conditions [*Raupach et al.*, 1997].

Following the calculation of the diagnostic variables within the stability loop, the prognostic variables are solved; the canopy water storage is then adjusted for dew and wet canopy fluxes and the soil model is solved for the current soil moisture and temperature, (see section 3.3). In the presence of snow on the ground, a snow model is used as described in detail in *Gordon et al.* [2002]. Finally, the carbon routines are called for the calculation of soil respiration and redistribution of the assimilation product between leaves, roots and wood. Soil respiration is a simple function of soil moisture and temperature. The flow of carbon between the vegetation and soil is described at present by a simple carbon pool model [*Dickinson et al.*, 1998]. This will be replaced in the version of CABLE used for ACCESS. The soil respiration formulation will also change as part of the new carbon pool scheme and hence the current scheme is not described in this report.

3.1.2 Formulation of aerodynamic resistances.

Energy and mass transfer exchange processes between land surfaces and the atmosphere occur over turbulent and laminar pathways. Localised Near Field (LNF) theory is used to describe the turbulent transfer within and above the canopy, see *Raupach* [1989a], *Raupach* [1989b].

LNF accounts for the fact that the eddies responsible for most scalar transfer in a canopy have a vertical length scale of the order of a large fraction of the canopy height. In the turbulent transfer the scalar concentration profile at height z in the air, $C(z)$, is related to the profiles of source strength, $S(z)$, and bulk vertical flux, $F(z)$. In LNF, $C(z)$ is comprised from the "far-field" and "near-field" components i.e. $C = C_f + C_n$. Two turbulence properties, vertical velocity standard deviation $\sigma_w(z)$, and Lagrangian time scale $T_L(z)$ are used to describe compliance of the "far-field" component with a gradient diffusion relationship between flux and concentration:

$$F(z) = -K_f(z)\frac{dC_f}{dz}, \tag{10}$$

$$K_f(z) = \sigma_w^2(z)\, T_L(z) \tag{11}$$

Parameterization of $\sigma_w(z)$ is a function of vegetation parameters such as height, h, and leaf area index over the whole grid cell, Λ, and the friction velocity, u_* (see section 3.5.1):

$$\sigma_w(z)/u_* = a_3^2 \, \min\left(\exp(\,c_{sw}\,\Lambda(z/h-1)\,),\ 1\right) \tag{12}$$

where a_3 is an aerodynamic parameter which gives the ratio of σ_w/u_* in the inertial sublayer and c_{sw} is a constant describing the rate of decrease of σ_w with depth.

Parameterization of $T_L(z)$ is more complex as it needs to account for different time scales of turbulence in the layer close to the ground i.e. below the zero-plane displacement d and below and above the roughness sublayer depth z_{ruf}:

$$T_L(z) = \begin{cases} k\,z\,/\,(\,a_3^2\,u_*\,\psi_H(\xi)\,) & z \geq z_{ruf} \\ f_{sp}(\Lambda)\,c_{TL}\,h/u_* & d \leq z < z_{ruf} \\ f_{sp}(\Lambda)\,c_{TL}\,h/u_*\,z/d & 0 \leq z < d \end{cases} \tag{13}$$

where k is the von Karman constant, ψ_H is the stability function for scalars, $f_{sp} = 1/\max\left(\frac{2}{3}\frac{d}{h}, 1\right)$ is a "sparseness factor" equal to 1 for dense canopy and approaching 0 as $\Lambda \rightarrow 0$, and c_{TL} is a constant (0.4). For detailed discussion on the formulation of $T_L(z)$ and σ_w see *Raupach et al.* [1997].

Using $\sigma_w(z)$ and $T_L(z)$, an expression for the turbulent aerodynamic resistance from a level z_x to the reference level z_{ref} is derived as:

$$r_x = \int_{z_x}^{z_{\text{ref}}} \frac{dz}{K_f(z)} = \int_{z_x}^{z_{\text{ref}}} \frac{dz}{\sigma_w^2(z)T_L(z)} \tag{14}$$

Integrating Eq.(14) over selected pathways gives aerodynamic resistances:

$$\begin{aligned} r_{ca} &= (\,\exp(2c_{sw}\Lambda(1-d/h))-1\,)\,/\,(a_3^2\,f_{sp}(\Lambda)\,c_{TL}2c_{sw}\Lambda) & d \leq z < h \\ r_{cb} &= dz\,/(a_3^2\,f_{sp}(\Lambda)\,c_{TL}\,h\,) & h \leq z < z_{ruf} \\ r_{cc} &= \tfrac{1}{k}\left[\,\ln(z_{\text{ref}}/(z_{ruf}-d)) - \psi_H(\xi) + \psi_H(\xi\,(z_{ruf}-d)/z_{\text{ref}})\right] & z_{ruf} \leq z < z_{\text{ref}} \end{aligned} \tag{15}$$

Total resistance in a single vegetation layer is:

$$r_{tc} = r_{ca} + r_{cb} + r_{cc} \tag{16}$$

The aerodynamic resistance from the soil to canopy is given by:

$$r_s = \ln\frac{z_{\text{ref}}}{z_0} \frac{\exp(2c_{sw}\Lambda) - \exp(2c_{sw}\Lambda(1 - d/h))}{a_3^2 \, f_{sp}(\Lambda) \, c_{TL} \, 2c_{sw}\Lambda} \tag{17}$$

Integrated stability functions, used to calculate aerodynamic canopy resistances and for the calculation of the friction velocity, use the Businger-Dyer form for unstable cases and the Webb form for stables cases, see *Paulson* [1970].
For scalar:

$$\psi_H(\xi) = \begin{cases} 2 \ln[\frac{1}{2}(1 + y)^2] & \text{with} \quad y = (1 - \gamma_h\xi)^{1/4} \quad \text{unstable} \\ -\beta\,\xi & \text{stable} \end{cases} \tag{18}$$

For momentum:

$$\psi_M(\xi) = \begin{cases} \ln\left[\frac{1}{4}(1 + x)^2\frac{1}{2}(1 + x^2)\right] - 2\arctan x + \frac{\pi}{2} & \text{with} \ x = (1 - \gamma_m\xi)^{1/4} \quad \text{unstable} \\ -\beta\,\xi & \text{stable} \end{cases} \tag{19}$$

and $\beta = 5$ and $\gamma_m = \gamma_h = 16$.

3.2 Canopy model

The canopy model calculates the exchange of radiation, heat, water and CO_2 between the land surface and the surface air of the atmosphere. It consists of canopy radiation, canopy turbulence and the coupled two-leaf model of photosynthesis-transpiration. Separate calculations for sunlit and shaded leaves are performed for photosynthesis, stomatal conductance, leaf temperature, energy and CO_2 fluxes. The distinction between sunlit and shaded leaves is important in scaling processes from leaf to canopy level as sunlit leaves receive much larger solar radiation fluxes than shaded leaves, and the response of photosynthesis to absorbed light is nonlinear.

3.2.1 Radiation transfer in plant canopies

The canopy in CABLE is placed above the ground allowing for full radiative coupling between the vegetation and the ground. The Goudriaan's model [*Goudriaan and van Laar*, 1994] was adopted by *Wang and Leuning* [1998] to calculate the interception, reflection, transmission and absorption by the plant canopy and soil.

The amount of radiation absorbed by sunlit and shaded leaves are calculated for three wavebands: visible (0.4 to 0.7 nm), near infra red (0.7 to 1.5 nm) and thermal radiation (> 10 nm).

The incoming short-wave radiation from the sun (S_0) is the sum of direct beam $(S_{b,j})$ and diffuse $(S_{d,j})$ radiation. That is:

$$S_0 = \sum_{j=1,2} (S_{b,j} + S_{d,j}), \tag{20}$$

where $S_{b,j}$ and $S_{d,j}$ represent the incident direct beam and diffuse radiation in the visible wave $(j=1)$ and near infra red $(j=2)$ waveband.

The total flux density of radiation within waveband j absorbed by the two big canopy leaves is calculated as

$$Q_{1,j} = \int_0^\Lambda q_{1,j}(\lambda) f_{sun}(\lambda)\, d\lambda \qquad \text{big sunlit leaf} \tag{21}$$

$$Q_{2,j} = \int_0^\Lambda q_{2,j}(\lambda)(1 - f_{sun}(\lambda))\, d\lambda \qquad \text{big shaded leaf} \tag{22}$$

where $\lambda \in [0, \Lambda]$ is the cumulative canopy leaf area index from the canopy top. The fraction of sunlit leaves within a canopy is calculated as $f_{sun} = \exp(-k_b\lambda)$, where k_b is the extinction coefficient of direct beam radiation for a canopy with black leaves described by Eq. 26.

The flux density of radiation absorbed by a sunlit $(q_{1,j})$ and shaded $(q_{2,j})$ leaf for visible (PAR) $(j = 1)$ or near infra red $(j = 2)$ (NIR) radiation in a canopy is calculated as:

$$q_{2,j}(\lambda) = (1 - \rho_{td,j})\, k_{d,j}^* \exp(-k_{d,j}\lambda) S_{d,j} + [(1 - \rho_{tb,j})\, k_{b,j}^* \exp(-k_{b,j}^*\lambda) - \tag{23}$$
$$(1 - \omega_j)\, k_b \exp(-k_b\lambda)] S_{b,j},$$
$$q_{1,j}(\lambda) = q_{2,j}(\lambda) + k_b(1 - \omega_j)\, S_{b,j}, \tag{24}$$

where $\rho_{tb,j}$ and $\rho_{td,j}$ are the surface (canopy and soil) reflectance for direct beam (b) and diffuse radiation (d) in waveband j, and $k_{b,j}^*$ and $k_{d,j}^*$ are the extinction coefficients (of direct beam and diffuse radiation in waveband j) in a real canopy, k_d and k_b are the extinction coefficients in a canopy with black leaves, and ω_j is the scattering coefficient of the leaf in waveband j. The extinction coefficients and surface reflectances are calculated according to *Goudriaan and van Laar* [1994]. $k_{b,j}^*$ and $k_{d,j}^*$ are related to the extinctions for a canopy with black leaves in the following way:

$$k_{b,j}^* = k_b(1 - \omega_j)^{\frac{1}{2}} \quad \text{and} \quad k_{d,j}^* = k_d(1 - \omega_j)^{\frac{1}{2}} \tag{25}$$

and

$$k_b(\theta) = \frac{G}{\cos(\theta)}, \tag{26}$$

$$k_d = -\frac{1}{\Lambda} \ln\left[\int_0^\Lambda \exp(-k_b(\theta)\lambda)\, d\lambda\right] \tag{27}$$

where G is the ratio of the projected area of leaves in the direction perpendicular to the direction of incident solar radiation and the actual leaf area. As an approximation, G can be calculated as

$$G = \phi_1 + \phi_2 \cos(\theta), \tag{28}$$
$$\phi_1 = 0.5 - 0.633\chi, \tag{29}$$
$$\phi_2 = 0.877(1 - 2\phi_1),$$

where χ is an empirical parameter related to the leaf angle distribution and $\chi = 0$ for spherical leaf angle distribution. The mean inclination angle decreases with an increase in χ. The above approximation for G is applicable for χ within the range of [-0.4, 0.6].

The effective canopy-soil reflectance is given by:

$$\rho_{tb,j} = \rho_{cb,j} + (\rho_{s,j} - \rho_{cb,j}) \exp(-2k_{b,j}^*\Lambda), \tag{30}$$
$$\rho_{td,j} = \rho_{cd,j} + (\rho_{s,j} - \rho_{cd,j}) \exp(-2k_{d,j}^*\Lambda), \tag{31}$$
$$\tag{32}$$

where $\rho_{s,j}$ is soil reflectance in waveband j, $\rho_{cb,j}$ and $\rho_{cd,j}$ are the reflectances of the canopy for direct beam and for diffuse radiation, respectively, at the top of the canopy, and are calculated as:

$$\rho_{cb,j} = \frac{2k_b}{k_b + k_d}\rho_{ch,j}, \tag{33}$$

$$\rho_{cd,j} = 2\int_0^{\pi/2} \rho_{cb,j}\sin(\theta)\cos(\theta)d\theta, \tag{34}$$

where $\rho_{ch,j}$ is the reflectance of a horizontally homogeneous canopy with black horizontal leaves, θ is the zenith angle of the sun.

The surface albedo for shortwave radiation for land is calculated as

$$\alpha_{land} = 0.5 \sum_{j=1,2} (\rho_{tb,j}f_b + \rho_{td,j}(1 - f_b)) \tag{35}$$

where f_b is the fraction of direct beam incoming short-wave radiation. If f_b, is not provided by the atmospheric radiation model, we use the empirical relationships developed by *Spitters* [1986] to estimate f_b. They are:

$$f_b = \begin{cases} 0 & 0.22 \le b_1 \\ 6.4(b_1 - 0.22)^2 & 0.22 < b_1 \le 0.35 \\ \min(1.66b_1 - 0.4728, 1) & b_1 > 0.35 \\ \max(1 - b_2, 0) & b_1 < b_2 \end{cases} \tag{36}$$

and

$$b_1 = \frac{S_0}{S_c(1 + 0.033\cos(2\pi(D_y - 10)/365))\cos(\theta)} \tag{37}$$

$$b_2 = (1.47 - b_3)/1.66 \tag{38}$$

$$b_3 = 0.847 + \cos\theta(1.04\cos(\theta) - 1.61) \tag{39}$$

where S_c is a solar constant ($S_c = 1370\,Wm^{-2}$) and D_y is a day of year.

The net long wave radiation balance of a leaf depends on leaf temperature which is calculated by solving the combined equations for leaf energy partitioning and photosynthesis (section 3.2.2). However, the solutions to the combined equations require the input of the net available energy, Rn_i, which includes the net long wave radiation. To overcome this difficulty, we calculate the net long wave radiation absorbed by the leaf under isothermal conditions (i.e. where leaf temperature $T_{f,i}$ is equal to air temperature T_a), and describe the difference in the absorbed long wave radiation between isothermal and non-isothermal conditions using radiative conductance (section 3.2.2).

The upwards and downwards long wave radiation flux densities within the canopy under isothermal conditions are calculated as:

$$L\!\uparrow(\lambda) = (1 - \exp(-k_d(\Lambda - \lambda)))L_f + \exp(-k_d(\Lambda - \lambda))L_s \tag{40}$$

$$L\!\downarrow(\lambda) = (1 - \exp(-k_d\lambda))L_f + \exp(-k_d\lambda)L_a \tag{41}$$

where L_a, L_f and L_s are the long wave radiation flux densities from sky, leaf under isothermal condition and soil, respectively, and are calculated from the Stefan-Boltzmann law:

$$L_a = \varepsilon_a\sigma T_a^4, \quad L_f = \varepsilon_f\sigma T_f^4, \quad L_s = \varepsilon_s\sigma T_s^4. \tag{42}$$

where ε_a, ε_f and ε_s are the emissivities and T_a, T_f and T_s are the temperatures of the sky, leaf and soil, respectively. The absorbed thermal radiation (wave band $j=3$) flux density by a leaf in the canopy ($q_{i,3}$) is then given by

$$q_{i,3} = \frac{d(L\!\uparrow - L\!\downarrow)}{d\lambda} = k_d\exp(-k_d(\Lambda - \lambda))(L_s - L_f) + k_d\exp(-k_d\lambda)(L_a - L_f) \tag{43}$$

The total flux density of absorbed long wave radiation by all sunlit leaves ($Q_{1,3}$) and shaded ($Q_{2,3}$) leaves are then given by

$$Q_{1,3} = \int_0^\Lambda f_{sun}(\lambda)q_{i,3}(\lambda)d\lambda = (L_s - L_f)k_d[\exp(-k_d\Lambda) - \exp(-k_b\Lambda)]/(k_d - k_b) \tag{44}$$

$$+ k_d(L_a - L_f)[1 - \exp(-(k_b + k_d)\Lambda]/(k_d + k_b)$$

$$Q_{2,3} = \int_0^\Lambda (1 - f_{sun}(\lambda))q_{i,3}(\lambda)d\lambda = (1 - \exp(-k_d\Lambda))(L_s + L_a - 2L_f) - Q_{1,3} \tag{45}$$

The net available energy for the big leaf i under isothermal conditions is calculated as

$$Rn_{c,i} = \sum_{j=1}^{3} Q_{i,j} \qquad i = 1,2 \tag{46}$$

3.2.2 The coupled model of stomatal conductance, photosynthesis and partitioning of net available energy

CABLE calculates photosynthesis, transpiration and sensible heat fluxes, separately for sunlit and shaded leaves. The distinction between sunlit and shaded leaves is necessary in scaling from leaf to canopy as the response of photosynthesis to the absorbed photosynthetically active radiation (PAR) is nonlinear.

Wang and Leuning [1998] compared the bulk formulation for the two leaf model with a multi-layered canopy model and found that the simulated fluxes of CO_2, water and sensible heat by the two leaf model agreed very closely with those from the multi-layered canopy model. The two-leaf model uses the same set of equations for calculating photosynthesis, transpiration and sensible heat fluxes for an individual leaf, but with the bulk formulation for the parameters for all sunlit and shaded leaves separately. For a given leaf parameter *P*, the corresponding parameter values for the two big leaves are calculated as

$$P_1 = \int_0^{\Lambda} p(\lambda) f_{sun}(\lambda) d\lambda \qquad \text{big sunlit leaf} \tag{47}$$

$$P_2 = \int_0^{\Lambda} p(\lambda)(1 - f_{sun}(\lambda)) d\lambda \qquad \text{big shaded leaf}$$

The basic set of equations for the coupled model of stomatal conductance, photosynthesis and transpiration for the big sunlit and shaded leaves is:

energy balance

$$Rn_{c,i} = \lambda E_{c,i} + H_{c,i}, \tag{48}$$

latent heat flux

$$\lambda E_{c,i} = \frac{sRn_{c,i} + c_p \rho_a D_a (G_{h,i} + G_{r,i})}{s + \gamma (G_{h,i} + G_{r,i})/G_{w,i}} \tag{49}$$

sensible heat flux

$$H_{c,i} = G_{h,i} c_p \rho_a (T_{f,i} - T_a), \tag{50}$$

stomatal conductance

$$G_{st,i} = \frac{G_{0,i}}{b_{sc}} + \frac{a f_w A_{c,i}}{C_{s,i}(1 + D_{s,i}/D_{s0)}}, \tag{51}$$

photosynthesis-gas diffusion

$$A_{c,i} = b_{sc}G_{st,i}(C_{s,i} - C_i) = G_{c,i}(C_a - C_i), \tag{52}$$

and photosynthesis-biochemistry

$$A_{c,i} = V_{n,i} - R_{d,i} \tag{53}$$

where

- $Rn_{c,i}$ is the net available energy partitioned into latent, $\lambda E_{c,i}$, and sensible, $H_{c,i}$, heat fluxes,

- D_a, T_a and C_a are vapour pressure deficit, temperature and CO_2 within the canopy space, respectively,

- Eq. 49 is a Penman-Monteith combination equation for latent heat flux, s is the slope of the curve relating saturation water vapour to temperature, and γ is psychrometric constant,

- in the Ball-Berry-Leuning model for stomatal conductance (Eq. 51), $G_{0,i}$ is stomatal conductance of a leaf for H_2O when net leaf photosynthesis is zero, $D_{s,i}$ is vapour pressure deficit at the leaf surface, f_w is an empirical parameter describing the availability of soil water for plants, and a and D_{s0} are empirical constants (the equation is applicable to C_3 and C_4 plants with different values of a, D_{s0} and $G_{0,i}$),

- in Eq. 52 describing supply of CO_2 by diffusion through stomata and the leaf boundary layers, $A_{c,i}$ is the net photosynthesis rate, $C_{s,i}$ is the CO_2 concentration at the leaf surface and C_i is intercellular CO_2 concentration of the leaf,

- in the biochemical demand equation (53), the net photosynthesis rate is calculated as the difference between net carboxylation rate of the big leaf $V_{n,i}$ and day respiration rate $R_{d,i}$. Carboxylation is the chemical reaction that reduces CO2 into carbonic acid. The reaction can be limited in two ways, by the availability of substrate, ribulose-1, 5-bisphosphate (RuBP-limited), or by the availability of the Rubisco enzyme, ribulose-1, 5-bisphosphate carboxylase-oxygenase, (Rubisco-limited),

- conductances $G_{w,i}$, $G_{h,i}$ and $G_{r,i}$ are for water, heat and radiation respectively, $G_{b,i}$ is boundary layer conductance and $G_{c,i}$ is total conductance for CO_2 from the intercellular space to the reference height; they are calculated as:

$$\text{water} \qquad G_{w,i}^{-1} = G_{a,i}^{-1} + G_{b,i}^{-1} + G_{st,i}^{-1} \tag{54}$$

$$\text{heat} \qquad G_{h,i}^{-1} = G_{a,i}^{-1} + (nb_{bh}G_{b,i})^{-1} \tag{55}$$

$$\text{boundary layer} \qquad G_{b,i} = G_{bu,i} + G_{bf,i} \tag{56}$$

$$\text{radiation} \qquad G_{r,i} = 4\,\varepsilon_f\sigma_b T_a^3 / c_p \tag{57}$$

$$\text{total} \qquad G_{c,i}^{-1} = G_{a,i}^{-1} + (b_{bc}G_{b,i})^{-1} + (b_{sc}G_{st,i})^{-1} \tag{58}$$

where $b_{bc} = 1.27$, $b_{sc} = 1.57$, $b_{bh} = 1.075$, and n=1 for amphistomatous leaves, and n=2 for hypostomatous ones. For a description of the calculation of boundary layer conductance $G_{b,i}$ see *Wang and Leuning* [1998]. The aerodynamic $G_{a,i}$ conductance is given by:

$$G_{a,i} = u_* / r_{tc}$$

where r_{tc} is described by Eq. 16. $G_{r,i}$ is the radiative conductance, see *Wang and Leuning* [1998].

3.2.3 An iterative method for the solution of the coupled canopy model equations.

The set of equations 48 to 53 has 6 unknowns; $T_{f,i}$, $D_{s,i}$, $C_{s,i}$, C_i, $A_{c,i}$, and $G_{st,i}$ which need to be calculated to obtain the photosynthesis ($A_{c,i}$), transpiration ($\lambda E_{c,i}$) and sensible heat flux ($H_{c,i}$) for a given set of atmospheric forcing and soil moisture conditions. Analytical solutions do not exist for all of the equations so an iterative method is required.

At the beginning of each time step we calculate aerodynamic and boundary layer resistances and the radiation absorbed by the canopy for the given meteorological forcing. As leaf temperature, $T_{f,i}$, is required for the calculation of the absorbed radiation energy, we approximate $Rn_{c,i}$ using the isothermal net radiation as described in Sec. 3.2.1:

$$Rn_{c,i} = R_{n,i}^* - c_p\, G_{r,i}(T_{f,i} - T_a) \tag{59}$$

where the last term describes the loss of thermal radiation of the big leaf under non-isothermal conditions. For the purpose of iteration we write the equations for the coupled model in the following way:

$$G_{st,i} = \frac{G_{0,i}}{b_{sc}} + \frac{af_w A_{c,i}}{C_{s,i}(1 + D_{s,i}/D_{s0})} \tag{60}$$

$$A_{c,i} = b_{sc}G_{st,i}(C_{s,i} - C_i) = G_{c,i}(C_a - C_i), \tag{61}$$

$$A_{c,i} = \min(V_{J,i}, V_{c,i}, V_{p,i}) - R_{d,i}, \tag{62}$$

$$\lambda E_{c,i} = \frac{sRn_{c,i} + c_p\rho_a D_a(G_{h,i} + G_{r,i})}{s + \gamma(G_{h,i} + G_{r,i})/G_{w,i}}, \tag{63}$$

$$R_{n,i}^* - c_p\, G_{r,i}\Delta T_i = \lambda Ec, i + H_{c,i} = \lambda Ec, i + c_p\rho_a G_{h,i}\Delta T_i, \tag{64}$$

$$D_{s,i}G_{st,i} = (D_a + s\Delta T_i)G_{w,i} \tag{65}$$

where $\Delta T_i = T_{f,i} - T_a$.

At the first iteration we set the leaf temperature to the air temperature at the reference level i.e. $T_{f,i} = T_a = T_{ref}$ and hence $\Delta T_i = 0$. $C_{s,i}$ and $D_{s,i}$ are set to the reference height values above the canopy i.e. C_a and D_a. The iteration method is as follows:

1. Eqs. 60 to 62 provide a description of photosynthesis. Given values of ΔT_i, $C_{s,i}$, and $D_{s,i}$ the equations can be solved analytically (see section 3.2.4) for the remaining three unknowns C_i, $A_{c,i}$ and $G_{st,i}$.

- the analytical solution for C_i requires evaluation of the photosynthetic parameters V_x (maximum rate of Rubisco-limited carboxylation) and J_x (maximum rate of potential electron transport). Both are dependent on leaf temperature $T_{f,i}$ as described in *Leuning* [2002]. Various other parameters related to photosynthesis and respiration are obtained before the calculation of C_i can be completed, see section 3.2.4.

- the analytic solution for C_i for the RuBP-limited and Rubisco-limited case is described by:

$$C_i = \frac{-b_1 + (b_1^2 - 4b_0b_2)^{1/2}}{2b_2} \tag{66}$$

and comes from the solution of the Eq. 89 which in turns come from the simultaneous solution of Eqs. 60, 61 and 62, as formulated by *Leuning* [1990]. For the description of b_i, where $i = 0, 1, 2$ see section 3.2.4.

- the carboxylation rates are evaluated separately for the RuBP-limited $V_{J,i}$, Rubisco-limited $V_{c,i}$ and sink-limited $V_{p,i}$ cases, see section 3.2.4.

- the net photosynthesis rate is calculated using the equation for biochemical demand for CO_2 (Eq. 62) which requires the minimum of the RuBP-limited, Rubisco-limited and sink-limited carboxylation rates.

- having generated a new value of the net photosynthesis, we compute the stomatal conductance $G_{st,i}$ using Eq. 60.

- Eq. 61 is rearranged to give a new value of $C_{s,i}$

$$C_{s,i} = C_i + (C_a - C_i)G_{c,i}/(b_{sc}G_{st,i}) \tag{67}$$

This completes the computation of the photosynthesis variables $A_{c,i}$, $G_{st,i}$, C_i and $C_{s,i}$.

2. Having computed $G_{st,i}$, the total conductance for water, $G_{w,i}$, is obtained from Eq. 54.

3. Penman-Monteith combination equation 63 is used for the canopy transpiration ($\lambda E_{c,i}$).

4. Sensible heat flux is calculated using Eq. 64.

5. Eq. 50 is now used to obtain a new value of leaf temperature $T_{f,i}$.

6. Eq. 65 gives a new value of $D_{s,i}$.

This completes the iteration for the 6 unknowns and evaluation of the fluxes of photosynthesis, transpiration and sensible heat. The new values of ΔT_i, $C_{s,i}$ and $D_{s,i}$ can now be used in the next iteration. The iteration is repeated until,

$$\mathrm{abs}(\Delta T_i^{iter+1} - \Delta T_i^{iter}) < 0.01 \tag{68}$$

see figure 1.

3.2.4   Description of the photosynthesis model

A description of the uptake of CO_2 by leaves requires a model for the CO_2 supply by diffusion from the ambient air to intercellular spaces and the demand for CO_2 by biochemical reactions of photosynthesis, Eq. 62. The net carboxylation rate in Eq. 62 is given by:

$$V_{n,i} = \min(V_{J,i}, V_{c,i}, V_{p,i}) \tag{69}$$

where $V_{J,i}$, $V_{c,i}$ and $V_{p,i}$ are the RuBP-limited, Rubisco-limited and sink-limited carboxylation rates. C_3 and C_4 plants have different photosynthetic pathways. Hence we present a description for each type before a mixed C_3/C_4 model is described.

a) C_3 plants

For C_3 plants, the RuBP-limited photosynthetic rate, $V_{3J,i}$, is calculated as

$$V_{3J,i} = \frac{J_i}{4} \frac{C_i - \Gamma^*}{C_i + 2\Gamma^*} \tag{70}$$

where Γ^* is the CO_2 compensation point in the absence of day respiration $(R_{3d,i} = 0)$, J_i is the electron transport rate and is given by the smaller positive root of the following quadratic equation:

$$\gamma_3 J_i^2 - (\alpha_3 Q_{3i,1} + J_{3x,i})J_i + \alpha_3 Q_{3i,1} J_{3x,i} = 0 \tag{71}$$

where γ_3 is an empirical parameter varying from 0 to 1, α_3 is the quantum efficiency of RuBP production and $J_{3x,i}$ is the maximum rate of potential electron transport (Eqs. 100 and 101) of the big leaf i at leaf temperature $T_{f,i}$. $Q_{3i,1}$ is the absorbed PAR (see Eqs. 21 and 22) ($Q_{3i,1} = (1 - c_4)Q_{i,1}$) and c_4 is a fraction of C_4 plants in the grid.

The Rubisco-limited photosynthetic rate for C_3 plants, $V_{3c,i}$ is calculated as

$$V_{3c,i} = \frac{V_{3x,i}(C_i - \Gamma^*)}{C_i + K_c(1 + O/K_0)} \tag{72}$$

where K_c and K_0 are the Michaelis-Menten constants for RuBP carboxylation and RuBP oxygenation respectively, O is the intercellular oxygen concentration and $V_{3x,i}$ is the maximum carboxylation rate (Eqs. 98 and 99) of leaf i at leaf temperature $T_{f,i}$.

The sink-limited photosynthetic rate, $V_{3p,i}$ for C_3 plants is calculated as

$$V_{3p,i} = 0.5V_{3x,i}. \tag{73}$$

Day respiration rate is calculated as

$$R_{3d,i} = 0.015V_{3x,i} \tag{74}$$

Respiration by leaves is included within the photosynthesis calculation while respiration by woody tissue and roots is dependent on temperature and the relevant carbon pool size. Details of the temperature dependence are given in *Wang et al.* [2006].

b) C$_4$ plants

RuBP-limited $V_{4J,i}$ is given by the smaller positive root of the following quadratic equation:

$$\gamma_4 V_{4J,i}^2 - (\alpha_4 Q_{4i,1} + V_{4x,i})V_{4,i} + \alpha_4 Q_{4i,1}V_{4x,i} = 0 \tag{75}$$

where γ_4 is an empirical constant, α_4 is the quantum efficiency of C$_4$ photosynthesis, $Q_{4i,1}$ is the absorbed PAR ($Q_{4i,1} = c_4 Q_{i,1}$), and $V_{4x,i}$ is the maximum carboxylation rate (Eqs. 102 and 103) of the big C$_4$ leaf.

The Rubisco-limited ($V_{4c,i}$) photosynthetic rate is calculated as

$$V_{4c,i} = V_{4x,i}. \tag{76}$$

The sink-limited carboxylation rate is calculated as:

$$V_{4p,i} = b_4 V_{4x,i} C_i \tag{77}$$

where b_4 is an empirical constant.

The day respiration rate of big leaf i is

$$R_{4d,i} = 0.025 V_{4x,i} \tag{78}$$

c) mixed C$_3$/C$_4$ model

Instead of applying the photosynthesis model for C$_3$ and C$_4$ plants separately we use the following formulation to calculate photosynthesis for a C$_3$/C$_4$ mixed grid cell (the formulation is also applicable to pure C$_3$ or C$_4$ grid cells).

When photosynthesis is either limited by Rubisco carboxylase or RuBP regeneration, Eq. 62 can be written in a more general form as

$$A_{c,i} = \frac{C_i - \Gamma^*}{C_i + C_{x,i}} V_{3,i} - R_i. \tag{79}$$

Note that subscripts J and c were dropped in $V_{3,i}$ as it represents both. For Rubisco carboxylase-limited photosynthesis rate, $V_{3,i}$, $C_{x,i}$ and R_i are given by

$$V_{3,i} = V_{4x,i}, \tag{80}$$
$$C_{x,i} = K_c(1 + O/K_0), \tag{81}$$
$$R_i = R_{3d,i} + R_{4d,i} - V_{4x,i}. \tag{82}$$

K_0, and K_c are functions of leaf temperature. For RuBP-limited photosynthesis rate, $V_{3,i}$, C_x and R are given by

$$V_{3,i} = \frac{J_i}{4},$$ (83)

$$C_{x,i} = 2\Gamma^*,$$ (84)

$$R_i = R_{3d,i} + R_{4d,i} - V_{4J,i}.$$ (85)

Γ^*, K_0 is a function of leaf temperature. Eq. 60 for stomatal conductance can be written for a C_3/C_4 mixed grid cell as

$$G_{st,i} = G_{0c} + XA_{c,i}$$ (86)

where

$$G_{0c} = (1 - c_4)G_{03} + c_4 G_{04}$$ (87)

$$X = \frac{(1 - c_4)a_3 f_w}{(C_{s,i} - \Gamma)(1 + D_{s,i}/D_3)} + \frac{c_4 a_4 f_w}{(C_{s,i} - \Gamma)(1 + D_{s,i}/D_4)}$$ (88)

where X is the so called Leuning constant. Eqs. 61, 79 and 86 can be solved analytically for $A_{c,i}$, C_i and $G_{st,i}$ for given values of $C_{s,i}$, $D_{s,i}$ and leaf temperature ($T_{f,i}$) [*Leuning*, 1990]. The analytic solution for C_i is given by the larger, positive root (Eq. 66) of the following equation:

$$b_2 C_i^2 + b_1 C_i + b_0 = 0$$ (89)

where

$$b_2 = G_{0c} + X(V_{3,i} - R_i)$$ (90)

$$b_1 = (1 - XC_{s,i})(V_{3,i} - R_i) + G_{0c}(C_{x,i} - C_{s,i}) - X(V_{3,i}\Gamma^* + C_{x,i}R_i)$$ (91)

$$b_0 = -(1 - XC_{s,i})(V_{3,i}\Gamma^* + C_{s,i}R_i) - G_{0c}C_{x,i}C_{s,i}$$ (92)

When photosynthesis is sink-limited, the carboxylation rate $V_{p,i}$ is calculated as:

$$V_{p,i} = 0.5V_{3x,i} + b_4 V_{4x,i}C_i$$ (93)

The above equation can be combined with Eq. 61 and 86 to solve for $A_{c,i}$, C_i and $G_{st,i}$, and $A_{c,i}$ is the smaller positive root of the following equation:

$$b_5 A_{c,i}^2 + b_6 A_{c,i} + b_7 = 0.$$ (94)

where

$$b_5 = X \tag{95}$$
$$b_6 = G_{0c} + b_4 V_{4x,i}(1 - XC_{s,i}) + X(R_d - 0.5V_{3x,i}) \tag{96}$$
$$b_7 = G_{0c}(b_4 C_{s,i} V_{4x,i} + 0.5V_{3x,i} - R_d) \tag{97}$$

The maximum carboxylation rate $V_{3x,i}$ and maximum rate of potential electron transport $J_{3x,i}$ for C_3 plants are calculated as:

$$V_{3x,1} = (1 - c_4)v_{c\ max,25} f_{vc\ max\ 3}(T_{f,1}) \int_0^\Lambda \exp(-k_b\lambda)\exp(-k_n\lambda)d\lambda \tag{98}$$

$$V_{3x,2} = (1 - c_4)v_{c\ max,25} f_{vc\ max\ 3}(T_{f,2}) \int_0^\Lambda (1 - \exp(-k_b\lambda))\exp(-k_n\lambda)d\lambda \tag{99}$$

$$J_{3x,1} = (1 - c_4)j_{max,25} f_{j\ max\ 3}(T_{f,1}) \int_0^\Lambda \exp(-k_b\lambda)\exp(-k_n\lambda)d\lambda \tag{100}$$

$$J_{3x,2} = (1 - c_4)j_{max,25} f_{j\ max\ 3}(T_{f,2}) \int_0^\Lambda (1 - \exp(-k_b\lambda))\exp(-k_n\lambda)d\lambda \tag{101}$$

The maximum carboxylation rate of C_4 plants, $V_{4x,i}$ is calculated as:

$$V_{4x,1} = (1 - c_4)v_{c\ max,25} f_{vc\ max\ 4}(T_{f,1}) \int_0^\Lambda \exp(-k_b\lambda)\exp(-k_n\lambda)d\lambda \tag{102}$$

$$V_{4x,2} = (1 - c_4)v_{c\ max,25} f_{vc\ max\ 4}(T_{f,2}) \int_0^\Lambda (1 - \exp(-k_b\lambda))exp(-k_n\lambda)d\lambda \tag{103}$$

where $f_{vc\ max\ 3}(T_{f,i})$, $f_{vc\ max\ 4}(T_{f,i})$, describe the temperature dependence of $v_{c\ max,25}$ for C_3 and C_4 plants. $f_{j\ max\ 3}(T_{f,i})$ describes the temperature dependence of maximum potential electron transport rate of C_3 plants. $v_{c\ max,25}$ and $j_{max,25}$ are the maximum carboxylation rate and maximum potential electron transport rate respectively for a leaf i. We assume $j_{max,25} = 2v_{c\ max,25}$.

3.3   Soil model

In order to simulate climate in GCMs, a realistic representation of soil temperature and moisture availability as well as their long term evolution is required. The soil model presented here has six layers and three prognostic variables namely, soil temperature, liquid water, and ice content. The amount of ice formed or melted is calculated from energy and mass conservation.

3.3.1   Soil Surface Energy Balance and Fluxes

Soil latent and sensible heat fluxes are obtained from the bulk transfer relations:

$$H_s = \rho c_p (T_s - T_{ref})/r_s, \tag{104}$$
$$\lambda E_{sp} = \lambda \rho (q^*(T_s) - q_{ref})/r_s, \tag{105}$$

where T_s is the soil surface temperature and r_s the resistance given by equation (17). E_{sp} is a potential evaporation which is the maximum possible evaporation from a surface under given atmospheric conditions and unlimited soil water supply. The Penman-Monteith combination equation [*Garratt*, 1992], provides an alternative formulation for the potential soil evaporation in the model. In this approach the combination of the energy and the aerodynamic contribution to evaporation is used as described by the first and second term, respectively:

$$\lambda E_{sl} = \Gamma(R_{Ns} - G_s) + (1 - \Gamma)\rho\lambda\delta q_d/r_s \tag{106}$$

where $\Gamma = s/(s+\gamma)$, s is $\partial q^*/\partial T$, $\gamma = c_p/\lambda$ the psychrometric constant, and δq_d is the humidity deficit in the air. R_{Ns} is the net radiative flux to the soil surface, and G_s is the heat flux into the soil.

For a wet surface $E_{sl} = E_{sp}$ while for a dry surface $E_{sl} < E_{sp}$, see [*Kowalczyk et al.*, 1991]. The actual evaporation from the soil surface is set to a fraction, x, of the potential evaporation E_{sp} or E_{sl}:

$$\lambda E_s = x\lambda E_{sp} \;\; or \;\; \lambda E_s = x\lambda E_{sl} \tag{107}$$

To calculate H_s and E_s, knowledge of soil surface temperature and moisture is required; we use values obtained at the previous timestep. The determination of the current time step surface temperature is based on the surface energy balance, which can be described as:

$$R_{Ns} - G_s = H_s + \lambda E_s \tag{108}$$

The net radiation at the soil surface comprises a combination of shortwave and longwave fluxes such that

$$R_{Ns} = (1-\alpha_s)S\downarrow + L\downarrow - \varepsilon_s L\uparrow \tag{109}$$

where $S\downarrow$ is the incoming shortwave radiation, $L\downarrow$ is the downward longwave flux and $L\uparrow = \sigma T_s^4$ is the upward longwave flux at the soil surface, α_s is the albedo and ε_s is emissivity of the surface. Flux G_s is given to the soil temperature diffusion equation (eq. 126) as the upper boundary condition (see section 3.3.4).

3.3.2　Soil moisture

The soil is a heterogeneous system composed of three constituent phases, namely the solid phase, water, and air [*Hillel*, 1982]. Water and air compete for the same pore space and continually change their volume fractions due to precipitation, evapotranspiration, snow melt and drainage. Soil hydraulic and thermal characteristics depend on the soil type as well as frozen and unfrozen soil moisture content. In this model, soil moisture is assumed to be at ground temperature, so there is no heat exchange between the moisture and the soil due to the vertical movement of water. Volumetric soil moisture, η, is considered in terms of liquid and ice components, $\eta = \eta_l + \eta_i$. Ice decreases soil porosity but liquid moisture can move through remaining unfrozen soil

pores. Each soil type is described by the following hydraulic characteristics: saturation content η_{sat}, wilting content η_w, and field capacity η_{fc}. η_{sat} is equal to the volume of all the soil pores which can fill with water under extremely wet conditions. Here, an additional variable, actual saturation η_{Asat} is used. Actual saturation excludes the pores filled with ice, $\eta_{Asat} = \eta_{sat} - \eta_i$.

The one-dimensional conservation equation for soil moisture in the absence of ice is described by

$$\frac{\partial \eta}{\partial t} = -\frac{\partial F}{\partial z} + r(z), \tag{110}$$

where F is the soil water flux and the r term includes runoff, drainage and root extraction for evapotranspiration. Water flux, F, in an unsaturated soil is given by Darcy's law

$$F = K - K\frac{\partial \psi}{\partial z} = K + D\frac{\partial \eta}{\partial z}, \tag{111}$$

where K is the hydraulic conductivity, ψ is the matric potential and $D = -K\partial\psi/\partial\eta$ is the diffusivity. Combining Eqs. 110 and 111 we obtain the Richard's equation

$$\frac{\partial \eta}{\partial t} = -\frac{\partial}{\partial z}(K + D\frac{\partial \eta}{\partial z}) + r(z). \tag{112}$$

To solve Eq.112 we need to assume forms of the relationship between the hydraulic conductivity, the matric potential, and the soil moisture content. The dependencies of *Clapp and Hornberger* [1978] are used,

$$K = K_s \left(\frac{\eta_l}{\eta_{Asat}}\right)^{2b+3}, \qquad \psi = \psi_s \left(\frac{\eta_l}{\eta_{Asat}}\right)^{-b} \tag{113}$$

where K_s and ψ_s are the values at saturation and b is a non-dimensional constant. η_{Asat} is calculated on the assumption that soil ice becomes part of the solid matrix. If we define the fractional liquid content as a function of actual saturation, $\eta_{lf} = \eta_l/\eta_{Asat}$ and substitute relations (113) into Eq. (112), we obtain the equation for the liquid water transfer in the soil:

$$\frac{\partial(\eta_{Asat}\,\eta_{lf})}{\partial t} = \frac{\partial}{\partial z}\left(K_s\psi_s\,b\,\eta_{lf}^{b+2}\frac{\partial \eta_{lf}}{\partial z} - K_s\,\eta_{lf}^{2b+3} \right) + r(z). \tag{114}$$

3.3.3 Solution of soil moisture equation

We first note that η_{Asat} may vary from timestep to timestep if the fraction of frozen soil alters. However, for the purposes of solving Richard's equation, (114), we need to assume that η_{Asat} remains constant during the timestep, whence a sequential solution in split manner gives the following pair of equations;
an advective equation

$$\eta_{Asat}\frac{\partial \eta_{lf}}{\partial t} + \frac{\partial}{\partial z}\left(K_s\eta_{lf}^{2b+3}\right) = 0 \tag{115}$$

and a diffusive equation including the sources and sinks

$$\eta_{Asat}\frac{\partial \eta_{lf}}{\partial t} = \frac{\partial}{\partial z}\left(K_s \psi_s b \eta_{lf}^{b+2}\frac{\partial \eta_{lf}}{\partial z}\right) + r(z). \tag{116}$$

The 6 soil layers have mid-layer depths $z_1, z_2, z_3, z_4, z_5, z_6$; the soil layers lie between the half-level depths $z_{0.5}, z_{1.5}, z_{2.5}, z_{3.5}, z_{4.5}, z_{5.5}, z_{6.5}$ with z defined as positive downwards.

Soil moisture vertical advection

Equation (115) has the nature of an advection equation in terms of η_{lf}, producing fluxes of $\eta_{Asat}\,\eta_{lf}$, with a downward advective "velocity", c, given by

$$c = \min\left(K_s \eta_{lf}^{2b+2}, \Delta z/\Delta t\right). \tag{117}$$

The velocities are calculated at the half-level interfaces at the current time τ, using the smaller of the neighbouring values of η_{lf} in order to avoid potential problems from isolated frozen soil layers, in which case η_{lf} will be very small. For numerical stability, it is imposed that the Courant number of the velocity is less than 1, which leads to the minimization condition in (117) involving Δz, the distance between the adjacent "full" levels; in particular for sand, c may become rather large due to the relatively large value of $K_s = 0.000166$ ms^{-1}.

Equation (115) is solved by the total variation diminishing (TVD) method. As discussed by *Durran* [1999], TVD methods avoid the growth of spurious ripples in the solution.

Low- and high-order fluxes are defined at the half-levels as follows. Noting that c is always positive downwards, the low-order flux is the first-order upstream expression

$$F_{k+1/2}^L = c_{k+1/2}\eta_{lf\_k}, \tag{118}$$

where, η_{lf_k} denotes η_{lf} with k subscript. The following high-order flux is used, based on the Lax-Wendroff method

$$F_{k+1/2}^H = \frac{c_{k+1/2}}{2}\frac{(z_{k+1}\eta_{lf\_k} + z_k\eta_{lf\_k+1})}{(z_{k+1} + z_k)} - \frac{c_{k+1/2}^2 \Delta t}{2}\frac{(\eta_{lf\_k+1} - \eta_{lf\_k})}{(z_{k+1} - z_k)}. \tag{119}$$

In the TVD method, these fluxes are combined using a flux-limiter, C, such that the net flux F is given by

$$F_{k+1/2} = F_{k+1/2}^L + C_{k+1/2}\left(F_{k+1/2}^H - F_{k+1/2}^L\right). \tag{120}$$

We choose to use the "superbee" flux limiter of *Roe* [1985],

$$C_{k+1/2} = \max\left[0, \min\left(1, 2s_{k+1/2}\right), \min\left(2, s_{k+1/2}\right)\right], \tag{121}$$

where

$$s_{k+1/2} = \left(\frac{\eta_{lf\_k} - \eta_{lf\_k-1}}{\eta_{lf\_k+1} - \eta_{lf\_k}} \right). \tag{122}$$

The smoothness variable $s_{k+1/2}$ represents the ratio of the slope of the solution upstream of $k+1/2$ to the slope of the solution across the interface at $k+1/2$ itself; s is approximately unity where the numerical solution is smooth [*Durran*, 1999], in which case the flux will be weighted towards the higher-order expression; s is negative when there is a local maximum or minimum immediately upstream of $k+1/2$, in which case $C_{k+1/2}$ becomes zero and the low-order flux is used. The final solution to (115) is given by

$$\eta_{lf\_k}^* = \eta_{lf\_k}^\tau - \Delta t \left(\frac{F_{k+1/2} - F_{k-1/2}}{z_{k+1/2} - z_{k-1/2}} \right) / \eta_{Asat\_k}^\tau, \tag{123}$$

where values at the current time step are denoted by superscript τ and those after this advective time step by $*$. Note that at the top and bottom half-levels, $z_{0.5}$ and $z_{6.5}$, the velocities and advective fluxes are set to zero.

There is an extra constraint applied to prevent soil layers from exceeding their saturated value. This is achieved by solving (123) from the lowest layer upwards; if for any layer this would lead to it being supersaturated, then the $F_{k-1/2}$ flux is reduced accordingly.

Soil moisture vertical diffusion

The diffusion equation 116 is also written in terms of half-level fluxes for $\eta_{Asat}\eta_{lf}$. It is solved for the current time step using as initial conditions η_{lf}^* from (123), as produced by the advection equation. In order to cope with the possibility of large diffusivities, implicit time differencing is used for the diffusion equation, leading to

$$\eta_{Asat}^\tau \frac{\left(\eta_{lf}^{\tau+1} - \eta_{lf}^* \right)}{\Delta t} = \frac{\partial}{\partial z} \left(K_s \psi_s b \eta_{lf}^{b+2} \frac{\partial \eta_{lf}^{\tau+1}}{\partial z} \right) + r^\tau(z). \tag{124}$$

The solution of this equation calculates fluxes at the half levels using diffusivities

$$\mathsf{K} = K_s \psi_s b \eta_{lf}^{b+2}$$

where the half-level η_{lf} are linearly averaged from the adjacent full-level values of η_{lf}^*. In finite difference form, (124) is expressed as

$$\frac{\eta_{Asat\_k}^\tau \eta_{lf\_k}^{\tau+1}}{\Delta t} - \frac{1}{(z_{k+0.5} - z_{k-0.5})} \left\{ \mathsf{K}_{k+0.5} \frac{\eta_{lf\_k+1}^{\tau+1} - \eta_{lf\_k}^{\tau+1}}{z_{k+1} - z_k} - \mathsf{K}_{k-0.5} \frac{\eta_{lf\_k}^{\tau+1} - \eta_{lf\_k-1}^{\tau+1}}{z_k - z_{k-1}} \right\}$$

$$= \frac{\eta_{Asat\_k}^\tau \eta_k^*}{\Delta t} + r_k^\tau. \tag{125}$$

This may be readily solved using a tridiagonal solver. The top and bottom boundary condition of zero diffusive fluxes is achieved by setting $\mathsf{K}_{0.5} = \mathsf{K}_{6.5} = 0$. The top layer includes r_1 terms that represent the flux infiltrating the surface which depends on rainfall, snowmelt, evaporation, surface runoff and soil hydrological properties. At the bottom, non-zero gravitational drainage acts towards restoring the water profile to its field capacity, via the term r_6.

3.3.4 Soil temperature

The vertical temperature profile is described by the following equation:

$$\rho_s c_s \frac{\partial T_s}{\partial t} = \frac{\partial}{\partial z}\left(\kappa_s \frac{\partial T_s}{\partial z}\right), \tag{126}$$

where ρ_s is the density $(kg\,m^{-3})$, c_s is the specific heat (J kg^{-1}K^{-1}) and κ_s is the thermal conductivity (W m^{-1} K^{-1}) of the soil. The volumetric heat capacity $(\rho_s c_s)$ is calculated as the weighted sum of the heat capacity of dry soil, liquid water and ice (air heat capacity is neglected),

$$\rho_s c_s = (1 - \eta_{sat})\,\rho_{dsoil}\,c_{dsoil} + \eta_l\,\rho_w\,c_w + \eta_i\,\rho_{ice}\,c_{ice}. \tag{127}$$

The soil dry density is estimated using soil porosity and assuming the same unit weight, ρ_{ws}, for solid components,

$$\rho_{soil} = (1 - \eta_{sat})\,\rho_{ws}. \tag{128}$$

Soil thermal conductivity κ_s plays a crucial role in determining the depth of freezing/thawing as it varies by about one order of magnitude as the soil approaches saturation point and increases further due to the ice content. A method for predicting κ_s in both frozen and unfrozen soils is based on *Johansen* [1975]. κ_s, is calculated as a combination of dry, κ_{dry}, and saturated, κ_{sat}, conductivities, weighted by a normalized thermal conductivity called the Kersten number,

$$\kappa_s = K_r\left(\kappa_{sat} - \kappa_{dry}\right) + \kappa_{dry}. \tag{129}$$

κ_{dry} is a function of the soil dry density. κ_{sat} depends on the soil porosity η_{sat}, the quartz content, and the liquid and ice volume fraction, whilst the Kersten number K_r is a simple function of saturation. The presence of water or ice in the soil can alter the soils thermal properties and thus modify soil temperature by several degrees. To take this into consideration the soil thermal properties are recalculated at each time step.

The bottom boundary condition for Eq. (126) is zero heat flow. At the top boundary the net heat flux at the surface is given by the G_s flux, see Eq. 108.

Following the solution of Eqs. (114) and (126) the freezing/thawing calculations are performed. If a soil layer temperature cools below freezing point and there is still unfrozen soil moisture, ice is formed. The amount of ice formed in a layer of thickness, δz, is limited by the amount of liquid water and available energy

$$\rho_w \, \delta z \, \delta \eta_i = \min \{ \rho_w \, \eta_l \, \delta z, \frac{(T_{frz} - T_s) \rho_s c_s \delta z}{L_f} \},$$ (130)

where L_f is the latent heat of fusion and T_{frz} is the freezing temperature. During freezing, latent heat is released from the soil and thus the soil is warmed. The layer temperature drops below freezing after all the water in the soil turns into ice. The melting process occurs when the temperature of a soil layer with ice increases to 0°C. The amount of ice melted is calculated in a similar fashion. In reality, the natural water in the soil and rocks freezes over a range of temperatures below 0°C.

4   Model simulations

To illustrate CABLE's capability in simulating diverse climatic conditions, we present examples of the model's simulations at three selected sites covered with vegetation: tropical rainforest, high latitude coniferous forest and Australian eucalyptus forest. The surface parameters for the sites are chosen not from the actual observed site descriptions, but from the C-CAM simulation with the resolution of 2x2°. At this resolution the model has only 13 vegetation types and 9 soil types with prescribed parameters relevant for each type.

The tropical rainforest site is in the Amazon Basin $(-4.6°, 299.5°)$. Figure 2 shows time series of various model variables for the period of 15 days in June obtained from the coupled C-CAM/CABLE simulation forced by observed sea surface temperatures. The site is characterised by the following parameters: leaf area index above 5 (plotted on panel j) as lai/10), tree height of 35 m and the soil type is clay.

Panel d) shows the partitioning of the available energy for the canopy into latent and sensible heat fluxes, with the latent heat flux composed of transpiration and wet evaporation (direct evaporation from the water stores on the canopy). In the Amazon basin, wet evaporation constitutes a significant part of the latent heat flux due to frequent precipitation events as depicted in panel e). In June precipitation is frequent but not large, as this is the beginning of the dry season which can be observed by the continuous decline in the moisture at all the soil levels, see panel g). Even with a decrease in precipitation, the major part of the available radiation is allocated to evapotranspiration as the tropical forest root system can access the deep soil moisture accumulated through the wet season.

Net radiation for soil is about 20% of that for the canopy due to canopy shading effects, (see panel f). Small latent heat flux and negligible sensible heat flux are due to the aerodynamic sheltering of the ground by the high forest with large LAI, resulting in most of the available net radiation going into soil ground heat flux. Diurnal amplitude of soil temperature is only up to about $6°C$, see panel h), and is smaller than the diurnal variation of air temperature depicted on panel b), due to shading and radiation effects of vegetation.

Carbon fluxes are depicted in panel i), with positive indicating a carbon source to the atmosphere. The model produces strong photosynthesis uptake and smaller fluxes of plant and soil respiration. Finally panel j) depicts a daily variation of calculated surface albedo.

The next two simulations are examples of offline use of CABLE, with the model being forced by the full set of atmospheric conditions which includes radiation fluxes, air temperature, humidity, wind speed, precipitation and surface pressure. The time series plots for January, April and June are simply intended to illustrate the model's behaviour and do not constitute a validation
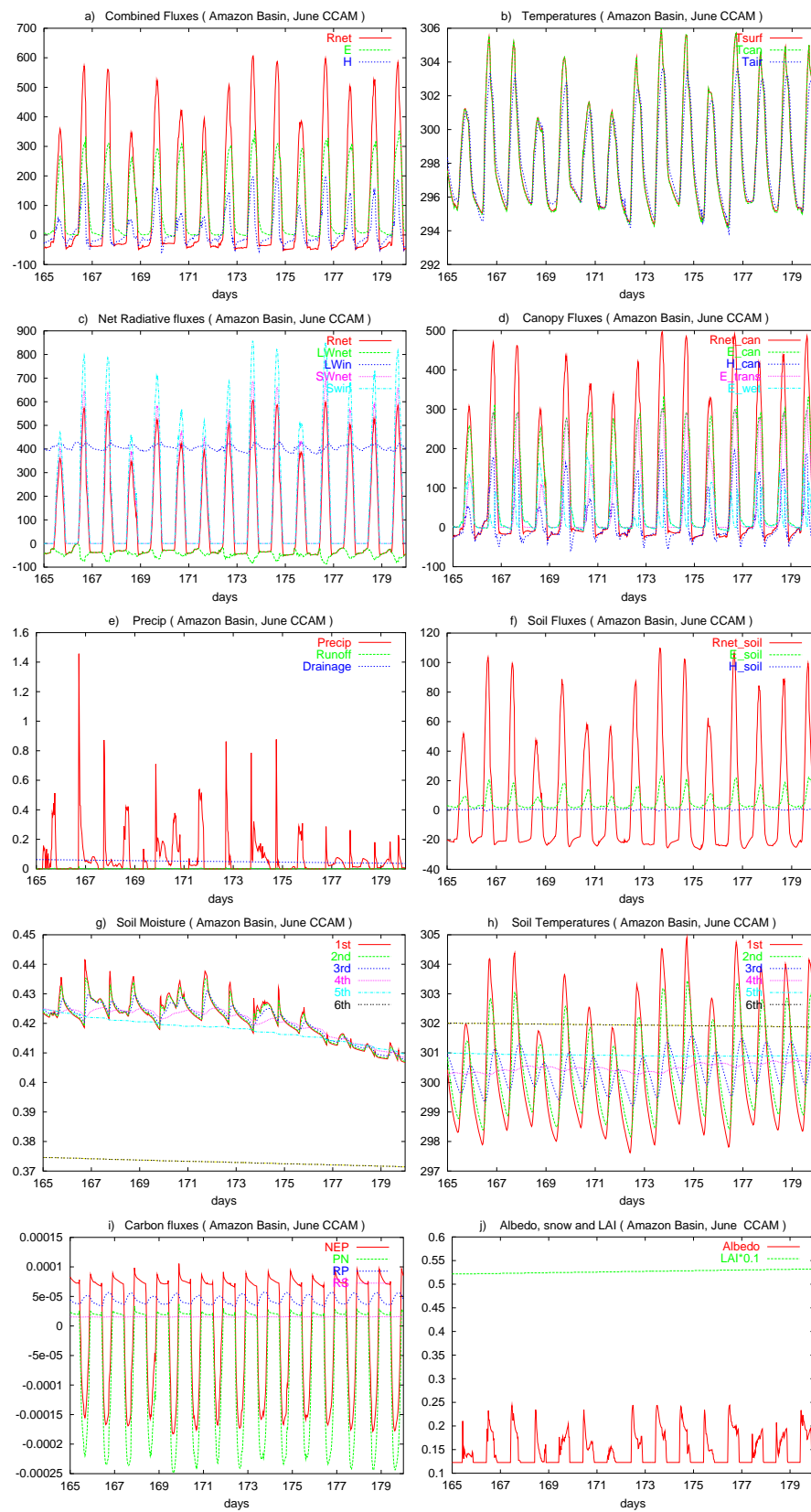
Figure 2: Timeseries of the modelled variables for tropical rainforest site in Amazon Basin.
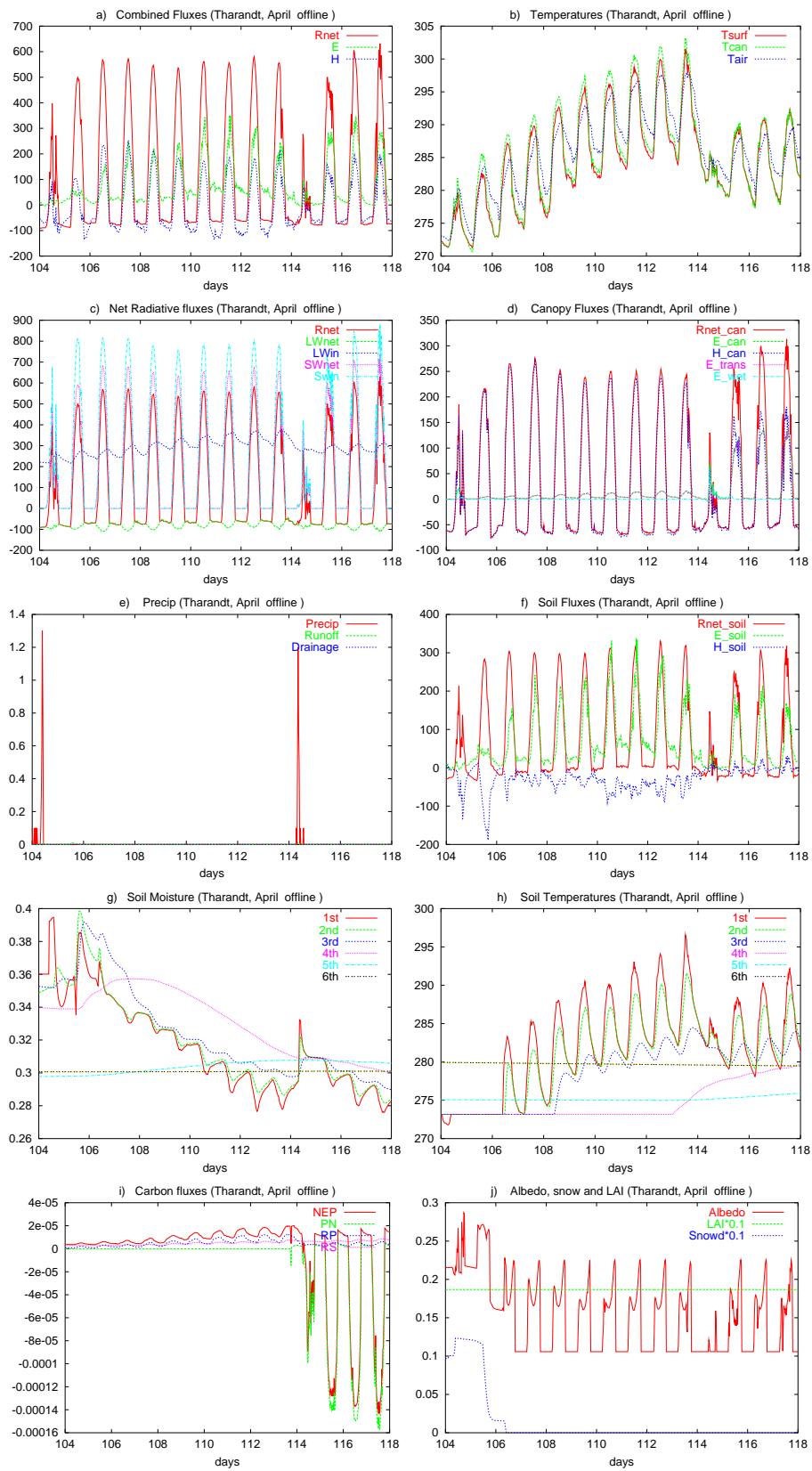
Figure 3: Timeseries of the modelled variables for coniferous forest in Tharandt.
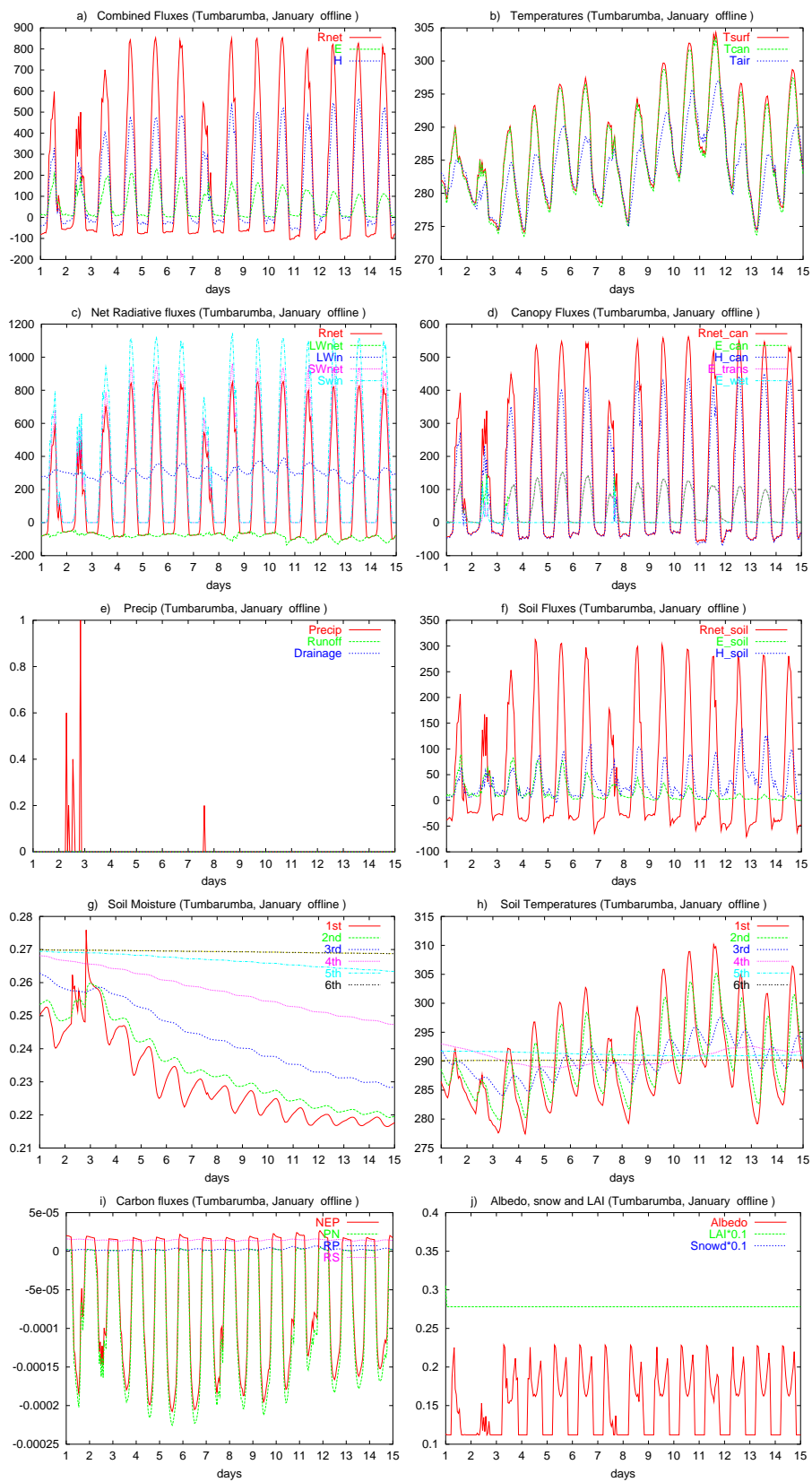
Figure 4: Timeseries of the modelled variables for eucalyptus forest site in Tumbarumba in January.
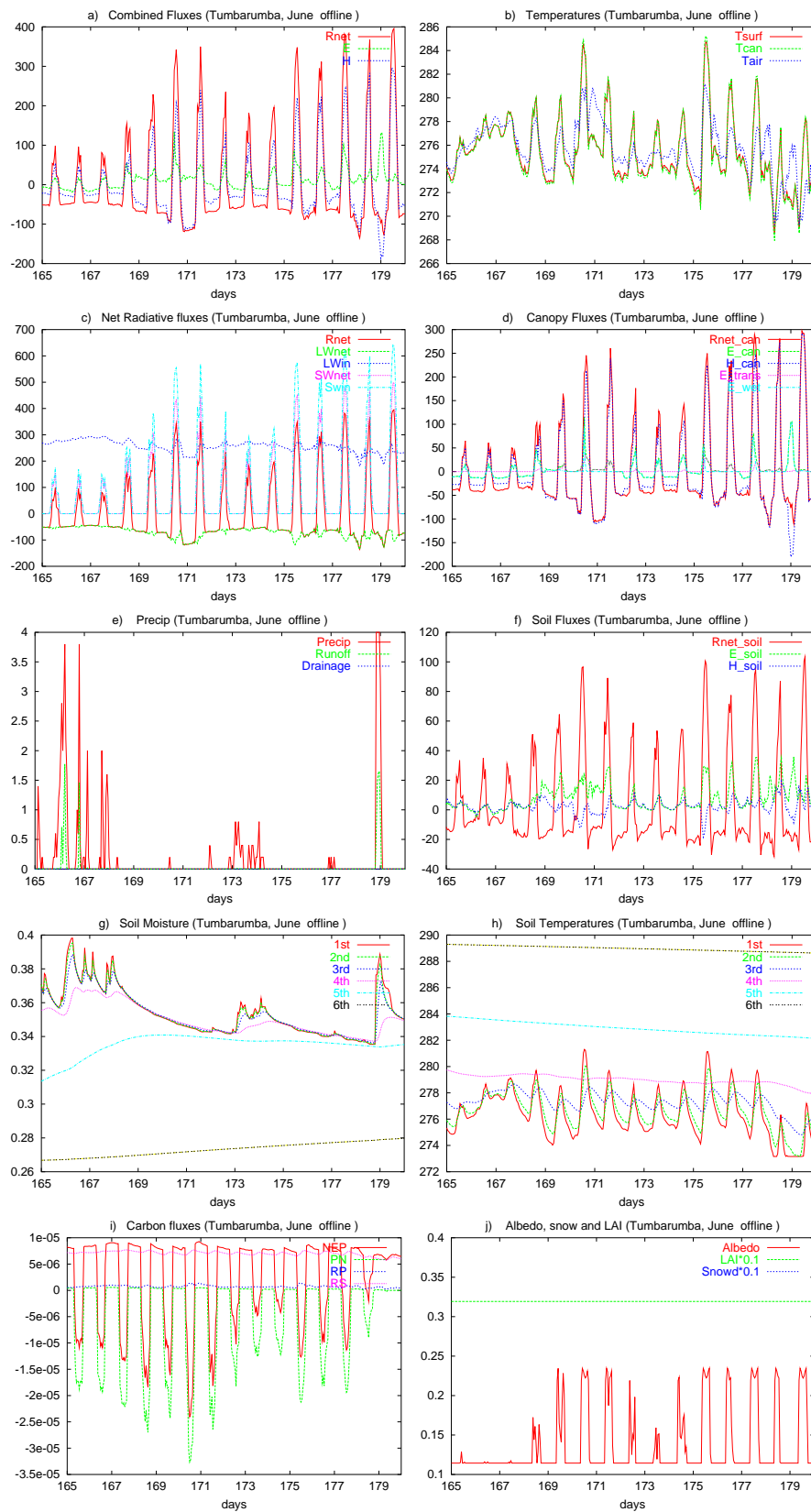
Figure 5: Timeseries of the modelled variables for eucalyptus forest site in Tumbarumba in June.
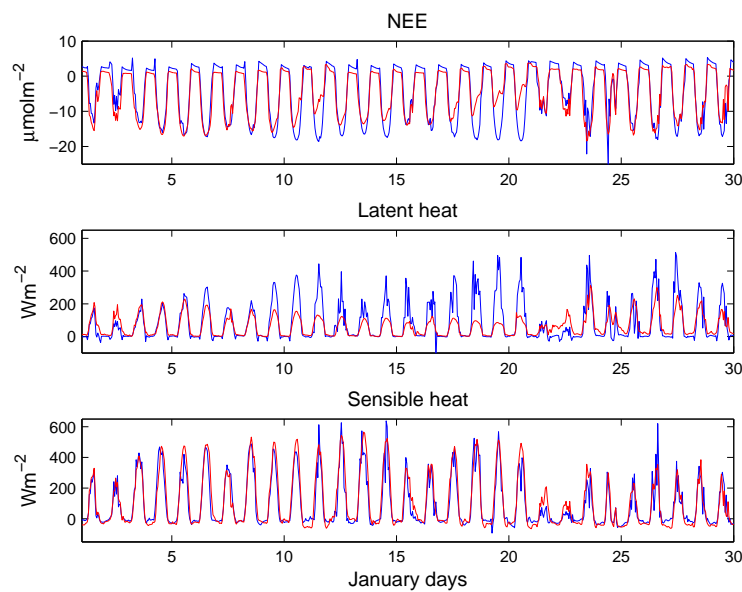
Figure 6: Timeseries of the observed (blue) and modelled (red) fluxes of a) the net biospheric CO_2 flux to the atmosphere b) latent heat flux and c) sensible heat flux for January 2002 at Tumbarumba.

of the model. CABLE's parameters and initial values for these simulations were taken from the same global fields as for the coupled run mentioned above. That is, each site's parameters were taken to be those representing the two by two degree grid box which contains the site. For each grid box initial model state values were derived from an equilibrium state of a coupled model simulation.

Half-hourly atmospheric forcing for the first site comes from the measurements at the eddy co-variance flux tower site in Tharandt, a coniferous forest site in north eastern Germany. Tharandt was prescribed as a needle-leaf evergreen tree site with medium clay soil type.

Tharandt meteorological input data was measured during 1996. Although in April the radiation fluxes are relatively high (see panel c), the snow still covers the ground reflecting back a part of the solar radiation. Panel j) shows the evolution of snow cover starting from a small snow depth, through fast snow melt due to above zero air temperatures (panel b) and rainfall (panel e) which accelerates melting of the snow. Soil moisture is frozen initially but unfreezes gradually with thawing snow and soil (panel g). The top two soil temperatures reached melting stage within two days, while the third and fourth layers melted four and nine days later respectively (panel h).

Panel d) shows the canopy available radiation partitioned to sensible heat flux and small evaporation flux. For the first ten days the transpiration flux is being inhibited by frozen soil but recovers in the last four days with the thawing of the ground. Similarly, carbon fluxes depicted on panel i) are initially composed of respiration followed by onset of photosynthesis.

Figure 4 shows January model output for Tumbarumba, a eucalypt forest site in south eastern Australia. The hourly meteorological input data to CABLE was measured at the flux towers during 2002. Tumbarumba's eucalyptus forest was represented in the coupled simulation as a broad-leaf evergreen tree site with medium clay soil. The prescribed canopy at Tumbarumba is not very dense (LAI 2.8) which allows a large portion of the incoming solar flux (depicted in
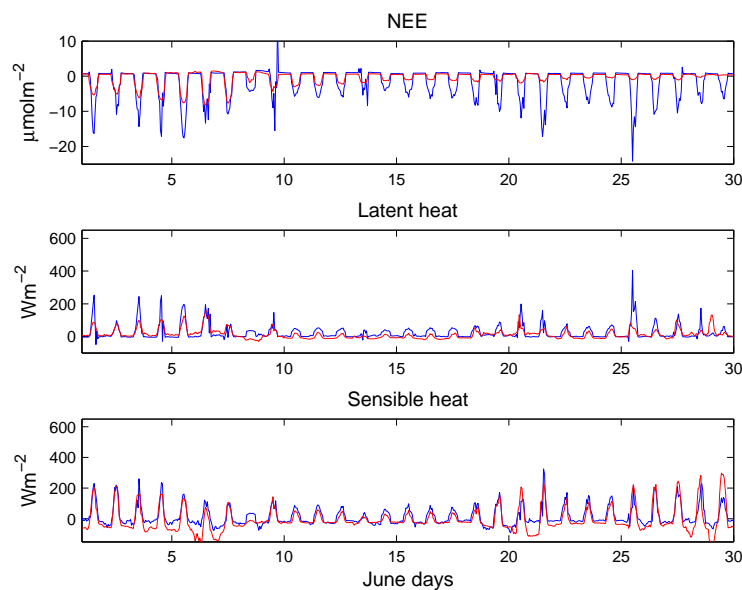
Figure 7: Timeseries of the observed (blue) and modelled (red) fluxes of a) the net biospheric CO_2 flux to the atmosphere b) latent heat flux and c) sensible heat flux for June 2002 at Tumbarumba.

panel c) to be transmitted down to the ground under the canopy. Net available radiation at the ground is around $250\,W/m^2$ (panel f), with a small portion partitioned to sensible heat flux, very little to latent heat flux due to water stress conditions, and the rest going to the ground heat flux. The latent heat flux becomes significant only following rainfall events.

A large part of the solar radiation is intercepted by the canopy giving large net radiation at the canopy surface. Most of this flux is partitioned to the sensible heat flux due to dry soil conditions depicted in panel g).

Soil surface temperatures are higher during the day than air temperature (panel h and b respectively) due to less effective shading of the canopy than at the Amazon Basin site, and dry soil conditions. Photosynthesis activity, depicted on panel i), is still large but decreases gradually with drying of the soil.

The June plot depicts much cooler conditions at the site with air temperatures gradually declining and attenuating the photosynthetic activity in spite of significant amounts of soil moisture available after the heavy rainfall early in the month,(see panel g). Soil temperatures are also cooling down (see panel h) while soil moisture is being replenished.

Using flux tower data allows us to compare CABLE's behaviour to observations at a high temporal resolution. Figures 6 and 7 shows January and June at Tumbarumba, with three modelled fluxes (shown in red) plotted against observations (shown in blue): latent heat, sensible heat, and net ecosystem exchange of CO_2. For the most part, CABLE provides a good qualitative fit for these fluxes. While quantitative measures across the entire simulation may seem more revealing, we avoid any in depth analysis here, as the parameters used to describe surface characteristics do not approximate the observations well enough.

Offline CABLE has been tested for many sites covering several continents and for a range of climatic and vegetation types. During these tests qualitative and quantitative comparisons were made, with quality controlled, gap-filled data from a number of flux tower sites [*Abramowitz,*

2005; *Wang et al.*, 2006].

4.1 Climate-carbon feedback simulations.

The carbon fluxes, photosynthesis (A_n), leaf respiration (R_d), plant respiration (R_p) and soil respiration (R_s), are output each timestep by CABLE. These fluxes can be aggregated in time to provide estimates of gross primary production, Φ_{GPP}, net primary production, Φ_{NPP}, and net ecosystem production, Φ_{NEP}.

$$\Phi_{GPP} = A_n + R_d \tag{131}$$

$$\Phi_{NPP} = A_n - R_p \tag{132}$$

$$\Phi_{NEP} = A_n - R_p - R_s \tag{133}$$

The fluxes can also be used to model atmospheric CO_2 when coupled to C-CAM or another atmospheric model.

The net biospheric flux to the atmosphere is $\Phi_{NEE} = R_p + R_s - A_n$. Flux units are $gCm^{-2}s^{-1}$. Flux is input to the lowest model level and converted to a change in concentration in the surface layer, ΔC in ppm, using

$$\Delta C = \frac{1000 \, \Phi_{NEE} \, g \, \Delta t \, M_{air}}{M_C \, \Delta\sigma \, p_s} \tag{134}$$

where g is the acceleration due to gravity, Δt is the model timestep (s), $\Delta\sigma$ is the fraction of the atmospheric column that makes up the lowest model level, p_s is surface pressure (Pa), M_{air} and M_C are the molecular masses of 'air' and carbon respectively.

After input to the atmosphere, the CO_2 is transported as a passive tracer, being subject to advection by the resolved winds and sub-grid scale transport by convection. Providing other components of the carbon cycle such as fossil emissions and ocean exchange are also modelled or prescribed, the total modelled CO_2 concentration can be used as input to CABLE and/or to C-CAM's radiation scheme. This enables climate-carbon feedbacks to be assessed but this has not been done for the fully coupled system. However, two preliminary tests have been performed. The first followed the C4MIP Phase 1 experimental protocol and used observed global CO_2 for both CABLE and the radiation scheme. The experiment is described in *Law et al.* [2006] and briefly below. The second used the modelled CO_2 for CABLE but used the prescribed global CO_2 for the radiation scheme.

The C4MIP experiment simulated the twentieth century using prescribed sea surface temperatures and global CO_2. This ensured a climate simulation with close to observed trends. CABLE responded to the increasing CO_2 and changing climate with increased Φ_{GPP}, Φ_{NPP} and respiration across the century (Fig. 8). At the end of the century the Φ_{NEE} was a small sink of CO_2 out of the atmosphere. The modelled atmospheric CO_2 was assessed for the last four decades of the simulation. A detailed presentation of the results is given in *Law et al.* [2006]. Here we summarise the main features. The results showed a reasonable simulation of the CO_2 growth rate over the last two decades. The seasonal cycle of CO_2 (first detrended using a smoothing spline) was well simulated in the northern high latitudes (e.g. Barrow, Alaska, Fig. 9a) but underestimated at mid-latitudes (e.g. Ulaan Uul, Mongolia, Fig.9b). There are limited sampling sites in the tropics but the seasonality at Cape Rama, India, a location strongly influenced by the monsoon, was well simulated (Fig. 9c). Seasonal cycles are small in the southern hemisphere but the phasing was incorrect at all sites (e.g. South Pole, Fig. 9d). The north-south CO_2 gradient was overestimated due to a northern mid-high latitude biospheric source and a southern low-mid latitude biospheric sink. A small sample of diurnal cycles suggested that respiration fluxes are too large, at least at the sampled locations. The final 40 years of the C4MIP experi-
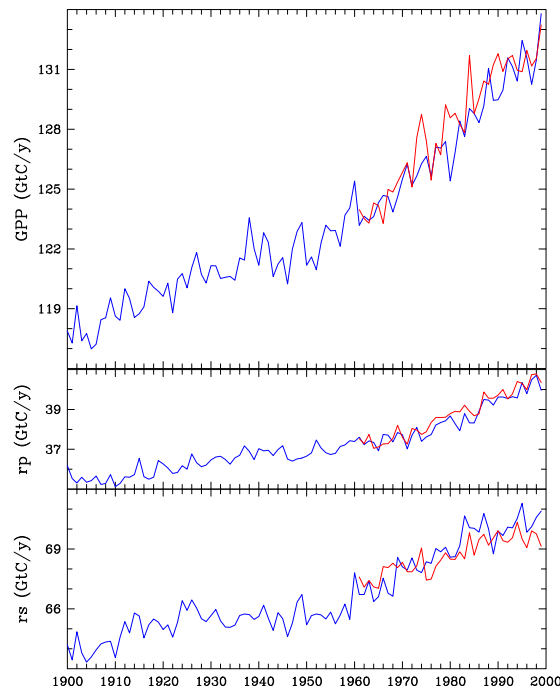
Figure 8: Gross primary production (Φ_{GPP}) (top), plant respiration (R_p) (middle) and soil respiration (R_s) (bottom) for the C4MIP simulation (blue) and the simulation in which CABLE was forced with variable CO_2 (red).

ment were repeated with CABLE forced by modelled rather than prescribed CO_2. The global growth rate of CO_2 can be approximated by the results from a single, remote site such as Mauna Loa, Hawaii. In the first decade of the simulation forced with modelled CO_2, the Mauna Loa CO_2 concentration increased more rapidly than in the C4MIP experiment (Fig. 10). However, from about 1975 the growth rate decreased and by 2000, the atmospheric CO_2 was about 12 ppm lower than in the C4MIP case (and closer to observed concentrations). This can be explained by looking at the carbon fluxes (Fig. 8). Each carbon flux increases over the century and shows interannual variability. Φ_{GPP} (photosynthesis) from the variable CO_2 run is larger than from the C4MIP run for the 1970s and 1980s. This is because photosynthesis increases as atmospheric CO_2 increases (the so-called "fertilization effect") and during the 1970s and 1980s the run using modelled CO_2 has higher concentrations than those prescribed in the C4MIP run. Note that the prescribed concentrations in the C4MIP run are based on observed concentrations and are lower than the modelled concentrations in the C4MIP case. The larger Φ_{GPP} fluxes in the 1970s and 1980s create an increased sink for atmospheric CO_2. This contributes to a slowing of the CO_2 growth rate and the return of CO_2 concentrations to observed levels. Consequently in the 1990s the Φ_{GPP} fluxes are similar for both simulations.

Plant respiration (R_p, Fig. 8b) shows similar behaviour although both the fluxes and the flux differences are smaller in magnitude. Plant respiration does not respond to atmospheric CO_2 directly, but rather to increasing plant pool sizes which are determined by Φ_{GPP}. The results for soil respiration (R_s) are harder to explain. Fig. 8c shows that R_s is initially larger in the variable CO_2 case than in the C4MIP simulation and then becomes smaller than the C4MIP values. Soil respiration is driven by soil temperature and moisture as well as the fast carbon pool size. In the variable CO_2 case, the fast carbon pool decreases slightly in the early 1960s then increases through the rest of the simulation. This would imply that R_s fluxes are opposite
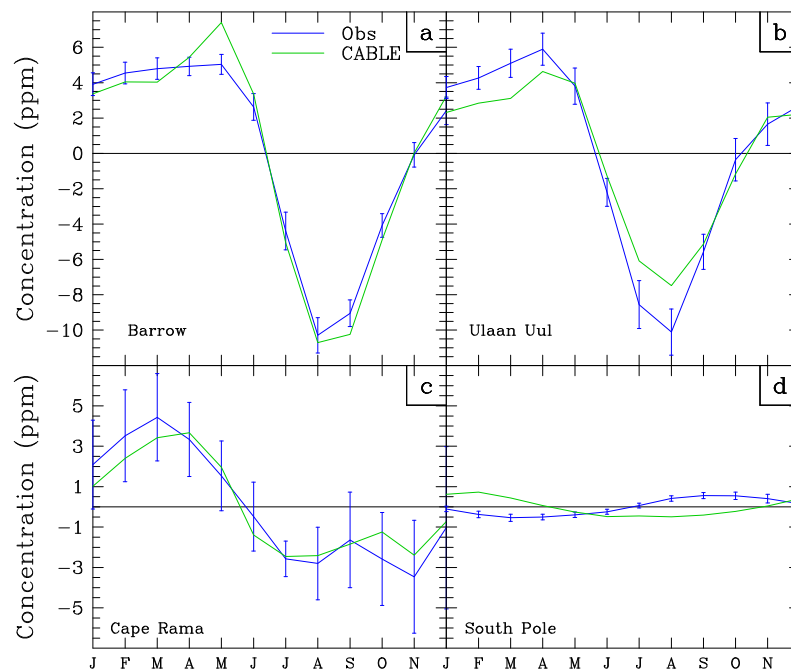
Figure 9: Observed (blue) and modelled (green) seasonal cycle of atmospheric CO_2 for four sites, Barrow (157^oW, 71^oN) (a), Ulaan Uul (111^oE, 44^oN) (b), Cape Rama (74^oE, 15^oN) (c) and South Pole (d). Model results for CABLE also include fossil, land-use and ocean contributions to seasonality. The interannual variability in the observed seasonal cycle is shown by the blue error bars.
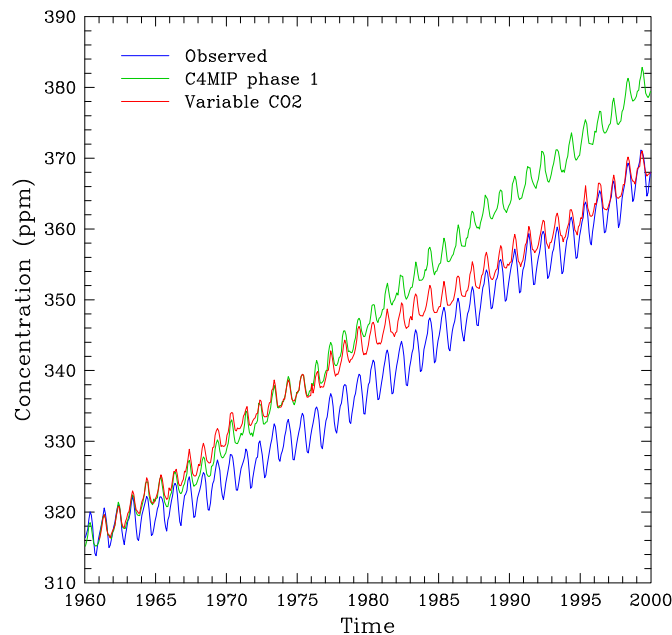
Figure 10: Observed (blue) and modelled atmospheric CO_2 concentration at Mauna Loa, Hawaii for the C4MIP simulation (green) and the simulation in which CABLE was forced with variable CO_2 (red).

to those obtained i.e. initially smaller than C4MIP and then larger. It is possible that trends in temperature and moisture dominate over the change in pool size, but there appears to be little evidence for significantly different trends in temperature and moisture between the two simulations. The C4MIP and the variable CO_2 simulations were performed many months apart with a 2003 version of C-CAM. It may be that a small change was made to the R_s formulation between the two simulations negating a clean comparison. In a future study, we plan to repeat these simulations with the current version of CABLE/C-CAM in order to check the results.

5 Final comments

We have described a biosphere atmosphere exchange model that forms the basis of a land surface scheme which is being incorporated into C-CAM and ACCESS GCMs. This model, together with surface data sets forms Phase I of a longer term plan to improve representation of surface processes in the CSIRO and ACCESS GCMs. Together with the basic description of the model, we have provided examples of the model performance.

6 Acknowledgments

References

Abramowitz, G., Towards a benchmark for land surface models, *Geophys. Res. Letts.*, *32*, L22,702, 2005, doi:10.1029/2005GL024419.

Clapp, R. B., and G. M. Hornberger, Empirical equations for some soil hydraulic properties, *Water resources research*, *14*, 601–604, 1978.

Deardorff, J. W., A parameterization of ground-surface moisture content for use in atmospheric prediction models, *J. Appl. Meteorol.*, *16*, 1182–1185, 1977.

Deardorff, J. W., Efficient prediction of ground surface temperature and moisture, with inclusion of a layer of vegetation, *J. Geophys. Res.*, *83*, 1889–1903, 1978.

Dickinson, R. E., M. Shaikh, R. Bryant, and L. Graumlich, Interactive canopies for a climate model, *J. Climate*, *11*, 2823–2836, 1998.

Durran, D., *Numerical methods for wave equations in GFD*, Springer Verlag, New York, 1999.

Finkele, K., J. J. Katzfey, E. A. Kowalczyk, J. L. McGregor, L. Zhang, and M. R. Raupach, Modelling of the OASIS energy flux measurements using two canopy concepts, *Boundary-Layer Meteor.*, *107*, 49–79, 2003.

Garratt, J. R., *The atmospheric boundary layer*, Cambridge University Press, 1992.

Gordon, H. B., et al., The CSIRO Mk3 Climate System Model, *CSIRO Atmospheric Research technical paper 60*, 2002, (electronic publication).

Goudriaan, J., and H. H. van Laar, *Modelling crop growth processes*, Kluwer, Amsterdam, The Netherlands, 1994.

Hillel, D., *Introduction to soil physics*, Academic Press, 1982.

Johansen, O., Thermal conductivity of soils, Ph.D. thesis, University of Trondheim, 1975.

Kowalczyk, E. A., J. R. Garratt, and P. B. Krummel, A soil-canopy scheme for use in a numerical model of the atmosphere - 1D stand-alone model, *CSIRO Division of Atmospheric Research technical paper 23*, 1991.

Kowalczyk, E. A., J. R. Garratt, and P. B. Krummel, Implementation of a soil-canopy scheme into the csiro gcm - regional aspects of the model response, *CSIRO Atmospheric Research technical paper 32*, 1994.

Law, R. M., E. A. Kowalczyk, and Y. P. Wang, Using atmospheric co_2 data to assess a simplified carbon-climate simulation for the 20th century, *Tellus*, *53B*, 427–437, 2006, doi:10.1111/j.1600-0889.2006.00198.x.

Leuning, R., Modelling stomatal behaviour and photosynthesis of *eucalyptus grandis*, *Aust. J. Plant Physiol.*, *17*, 159–175, 1990.

Leuning, R., Temperature dependence of two parameters in a photosynthesis model, *Plant Cell Environ.*, *25*, 1205–1210, 2002.

Leuning, R., F. M. Kelliher, D. G. G. De Pury, and E.-D. Schulze, Leaf nitrogen, photosynthesis, conductance and transpiration: scaling from leaves to canopies, *Plant Cell Environ.*, *18*, 1183–1200, 1995.

Louis, J. F., A parameteric model of vertical eddy fluxes in the atmosphere, *Bound. Layer Meteor.*, *17*, 187–202, 1979.

Monin, A. S., and A. M. Obukhov, Basic laws of turbulent mixing in the atmosphere near the ground, *Tr. Geofiz. Inst., Akad. Nauk SSSR*, *24*, 163–187, 1954.

Paulson, C. A., The mathematical representation of wind speed and temperature profiles in the unstable atmospheric surface layer, *J. Appl. Meteor.*, *9*, 857–861, 1970.

Raupach, M. R., Applying lagrangian fluid-mechanics to infer scalar source distributions from concentration profiles in plant canopies, *Agric. Forest Meteor.*, *47*, 85–108, 1989a.

Raupach, M. R., A practical lagrangian method for relating scalar concentrations to source distributions in vegetation canopies, *Quart. J. Roy. Meteor. Soc.*, *115*, 609–632, 1989b.

Raupach, M. R., Simplified expressions for vegetation roughness length and zero-plane displacement as functions of canopy height and area index, *Boundary-Layer Meteor.*, *71*, 211–216, 1994.

Raupach, M. R., K. Finkele, and L. Zhang, SCAM (Soil-Canopy-Atmosphere Model): description and comparison with field data, *CSIRO Centre for Env. Mechanics Tech. Rep. 132*, 1997.

Roe, P. L., Some contributions to the modelling of discontinuous flows, in *Lecture notes in Applied Mathematics*, vol. 22, pp. 163–193, Springer-Verlag, New York, 1985.

Spitters, C. J. T., Separating the diffuse and direct component of global radiation and its implication for modelling canopy photosynthesis. Part II: Calculations of canopy photosynthesis, *Agric. Forest Meteor.*, *38*, 231–242, 1986.

Wang, Y.-P., A refinement to the two-leaf model for calculating canopy photosynthesis, *Agric. Forest Meteor.*, *101*, 143–150, 2000.

Wang, Y. P., and R. Leuning, A two-leaf model for canopy conductance, photosynthesis and partitioning of available energy I. Model description and comparison with a multi-layered model, *Agric. Forest Meteor.*, *91*, 89–111, 1998.

Wang, Y.-P., D. Baldocchi, R. Leuning, E. Falge, and T. Vesala, Estimating parameters in a land-surface model by applying nonlinear inversion to eddy covariance flux measurements from eight FLUXNET sites, *Glob. Change Biol.*, *12*, 2006, doi:10.1111/j.1365-2486.2006.01225.x.